Reviewed Preprint
v1 • February 13, 2026
Not revised

Reviewed Preprint
v2 • April 20, 2026
Revised by authors

For correspondence:
Ying.Sun@cchmc.org

Competing interests: K.D.R.S. discloses outside this work equity in Asklepion Pharmaceuticals, Baltimore, and Aliveris s.r.l. Italy and is a consultant to Mirum Pharmaceuticals. Other authors declare no competing interests.

Funding: See page 22

Reviewing editor: Hugo J Bellen, Baylor College of Medicine, United States

Patient-Specific Midbrain Organoids with CRISPR Correction Recapitulate Neuronopathic Gaucher Disease Phenotypes and Enable Evaluation of Novel Therapies

Yi Lin[1], Benjamin Liou[1], Venette Fannin[1], Stuart Adler[1], Christopher N Mayhew[2,3], Jason E Hammonds[2,4], Yueh-Chiang Hu[2,5], Jason Tchieu[2,6], Wujuan Zhang[7], Xueheng Zhao[2,7], Rebecca L Beres[7], Kenneth DR Setchell[2,7], Ahmet Kaynak[8], Xiaoyang Qi[2,8], Ricardo A Feldman[9], Ying Sun[1,2]

[1]Division of Human Genetics, Cincinnati Children's Hospital Medical Center, Cincinnati, United States • [2]Department of Pediatrics, University of Cincinnati College of Medicine, Cincinnati, United States • [3]Pluripotent Stem Cell Facility & Developmental Biology, Cincinnati Children's Hospital Medical Center, Cincinnati, United States • [4]Division of Infectious Diseases, Cincinnati Children's Hospital Medical Center, Cincinnati, United States • [5]Transgenic Animal and Genome Editing Facility, Cincinnati Children's Hospital Medical Center, Cincinnati, United States • [6]Division of Developmental Biology, Cincinnati Children's Hospital Medical Center, Cincinnati, United States • [7]Division of Pathology and Laboratory Medicine, Cincinnati Children's Hospital Medical Center, Cincinnati, United States • [8]Division of Hematology/Oncology, Department of Internal Medicine, University of Cincinnati, College of Medicine, Cincinnati, United States • [9]Department of Microbiology and Immunology, University of Maryland School of Medicine, Baltimore, United States

eLife Assessment

This study provides potentially **important** insights by establishing a human disease model and exploring therapeutic approaches. The evidence is generally **convincing** for descriptive and comparative findings. The authors present **solid** data, but evidence for proposed biological mechanisms and functional outcomes remains limited.

https://doi.org/10.7554/eLife.109518.2.sa4

Abstract

Neuronopathic Gaucher disease (nGD) is a lysosomal storage disorder caused by *GBA1* mutations, leading to defective acid β-glucosidase (GCase) and accumulation of glycosphingolipid substrates, causing inflammation and neurodegeneration. Patients with nGD manifest severe neurological symptoms, but current animal models fail to fully recapitulate human condition, posing a major barrier to the development of effective therapies targeting the brain. To bridge this gap, we have developed midbrain-like organoids (MLOs) from human induced pluripotent stem cells (hiPSCs) of nGD patients with $GBA1^{L444P/P415R}$ and $GBA1^{L444P/RecNcil}$ mutations to model nGD brain pathogenesis. These nGD MLOs exhibited GCase deficiency, resulting in diminished enzymatic function, accumulation of lipid substrates, widespread transcriptomic changes, and impaired dopaminergic neuron differentiation, mirroring nGD pathology. *GBA1* mutation correction mediated by CRISPR/Cas9 restored GCase activity, normalized lipid substrate levels, and rescued dopaminergic neuron function, confirming the causal role of *GBA1* mutations during early brain development. Using this novel platform, we further evaluated therapeutic strategies, including SapC-DOPS nanovesicles delivering GCase, AAV9-GBA1 gene therapy, and substrate reduction therapy with GZ452, a glucosylceramide synthase inhibitor currently under clinical investigation. These treatments either restored GCase activity, reduced lipid substrate accumulation, improved

autophagic and lysosomal abnormalities, or ameliorated dysregulated genes involved in neural development. These patient-specific, 3D neural models offer a transformative, physiologically relevant platform for unravelling disease mechanisms and accelerating the discovery of therapies for patients with nGD.

Introduction

Gaucher disease (GD) is a lysosomal storage disorder caused by *GBA1* mutations, which impair acid β-glucosidase (GCase). Defective GCase leads to accumulation of its glycosphingolipid substrates, glucosylceramide (GluCer) and glucosylsphingosine (GluSph), triggering inflammation and neurodegeneration. GD affects 1/450 in Ashkenazi individuals and 1/50,000 globally [1]. There are three GD types: Type 1 present mainly visceral symptoms and is not life-threatening [1]. while neuronopathic GD (nGD, Types 2 and 3) involves severe neurological manifestations. Type 2 patients typically die by age 2, indicating early central nervous system (CNS) defects [2,3].

Current knowledge of brain pathogenesis in nGD is limited to a few postmortem brain analyses showing prominent neuronal loss and astrogliosis in the midbrain [4–6]. GD mouse models, including GCase knockout, irreversible GCase inhibitor conduritol B-epoxide (CBE) induced mouse models, double transgenic mutant model harboring both *Gba1* and Saposin C mutations (Saposin C is the activator of GCase), have been widely used to study disease pathogenesis and therapies [7–12]. These models replicate neuronal loss and astrogliosis [4–6,8,13], but have limitations. The knockout and CBE-induced models lack *GBA1* mutations, and the double transgenic model has a second gene that may change the GD phenotype, and knock-in models fail to mimic human phenotypes [10,14]. For example, mice with the $Gba1^{L444P/L444P}$ or $Gba1^{D409H/D409H}$ mutations show no neuronopathic disease despite <10% of residual GCase activity [10,14–16]. These constraints highlight the need for physiologically relevant human nGD models.

Brain organoids derived from human induced pluripotent stem cells (hiPSC) emerged as a powerful 3D model to study brain development and CNS diseases [17]. Unlike 2D monolayer neural cells, brain organoids contain diverse neural and glial cell types arranged in 3D comprising subventricular zone and multiple organized cellular layers that more closely represents the spatial architecture of the human brain [18]. They have been used to study neurodegenerative and lysosomal diseases, including Parkinson's disease (PD), Alzheimer's disease, and Sandhoff disease [19–23]. A brain organoid derived from hiPSCs of a healthy individual with *GBA1* knockout and α-synuclein overexpression exhibited characteristic PD markers [24]. However, this model lacks patient-specific *GBA1* mutations needed for clinical relevance. To develop a relevant model, we developed novel midbrain organoids from nGD patients with *GBA1* mutations, a model not yet well studied.

The midbrain region is prominently affected in nGD [4–6]. Patients with nGD often exhibit impaired vertical gaze and movement disorders. These symptoms correlate with midbrain involvement due to the sensitivity of this region to neuroinflammatory and degenerative processes [4,25]. Both human and mouse studies indicate that the midbrain shows prominent substrate accumulation compared with other brain regions, suggesting it is particularly susceptible to pathological burden in GD midbrain [4,26–28]. To model the midbrain-specific disease, we derived midbrain-like organoids (MLOs) from Type 2 patient-derived hiPSCs carrying either $GBA1^{L444P/P415R}$ or $GBA1^{L444P/RecNcil}$ mutations. These GD MLOs showed reduced GCase activity, lipid substrate accumulation, transcriptomic alterations, and impaired dopaminergic neuron differentiation. CRISPR/Cas9-mediated correction of *GBA1* mutation confirmed the causal role of *GBA1* mutations in these phenotypes and mitigated disease phenotypes. To explore therapeutic potential, we tested three emerging treatments in GD MLOs: CNS accessible enzyme therapy (SapC-DOPS-GCase), gene therapy (AAV9-GBA1) and substrate reduction therapy (GZ452). Our results demonstrate the utility of patient-derived MLOs for studying nGD pathogenesis and advance drug development.

Materials and Methods

Maintenance of hiPSCs and generation of MLOs

Three hiPSCs lines (WT-75.1, GD2-1260 and GD2-10-257) generated previously [29,30] (Supplementary Table 1) were maintained in mTeSR1 complete medium (StemCell) on six-well plates coated with Vitronectin (1:100 diluted in DPBS, 1 mL/well, incubated at RT for 1 hour). HiPSCs at ~70% confluency were treated and replated at 1:20 to 1:60 ratios, with optional 10 μM ROCK inhibitor (Y-27632, StemCell) for survival. All hiPSC lines were authenticated using short tandem repeat (STR) profiling and were verified as mycoplasma-free.

MLO generation method was modified based on published protocol [31,32]. Briefly, hiPSCs were pretreated with 50 μM Y-27632 for 1 hour, dissociated with Accutase (Millipore-Sigma) into singlets, centrifuged (200 × g, 5 minutes), and resuspended in embryoid body (EB) medium (EBM; consisting of DMEM/F12, 20% KnockOut Serum Replacement (KSR), 1% penicillin/streptomycin, GlutaMAX, NEAA, 55 μM β-mercaptoethanol, 1 μg/mL heparin, 3% FBS, 4 ng/mL bFGF, 1× CEPT). For each organoid, 1.2~1.5 × 10^4 hiPSC cells were seeded in 100 μL EBM per well in ultra-low attachment (ULA) U-bottom 96-well plates, centrifuged at 500 × g for 3 minutes, and incubated at 37°C, 5% CO_2; on day 2, 150 μL EBM with 4 ng/mL bFGF (no ROCK inhibitor) was added. Once the EBs grow to 400 to 475 μm in size, they were transferred to a new ULA 96-well plate with 125 μL brain organoid generation medium (BGM, consisting of 50% DMEM/F12, 50% Neurobasal, 1× N2, 1× B27 without vitamin A, 1% penicillin/streptomycin, 1% GlutaMAX, 1% NEAA, 55 μM β-mercaptoethanol, 1 μg/mL heparin) supplemented with dual SMAD inhibitors (SMADi: 2 μM dorsomorphin, 2 μM A83-01, 3 μM CHIR99021, 1 μM IWP2), refreshed every other day until day 11. On day 7 or 8, mesencephalic floor plate induction was initiated by adding 125 μL BGM containing 1× SMADi, 100 ng/mL FGF8, and 2 μM SAG until day 16. On day 11, four EBs were transferred to one well of ultra-low attachment 24-well plates with 500 μL BGM-MLOs induction medium, consisting of BGM with 100 ng/mL FGF8, 2 μM SAG, 200 ng/mL laminin, 2.5 μg/mL insulin, 2% Growth Factor Reduced (GFR) Matrigel, and refreshed with Matrigel on day 14. On day 16, three MLOs per well were transferred to ultra-low attachment 6-well plates in brain organoid maturation medium (BGM-BMM), consisting of BGM with 10 ng/mL BDNF, 10 ng/mL GDNF, 200 μM ascorbic acid, 125 μM db-cAMP, 1% GFR Matrigel, cultured on an orbital shaker (100 rpm) to reduce spontaneous fusion with medium changes every 3 days. Starting at day 30, GFR Matrigel was removed, and brain organoids were cultured solely in BGM medium till the date of analysis.

Immunostaining and image analysis of sectioned MLOs

Organoids were washed with 1xDPBS and fixed in 4% paraformaldehyde (PFA) overnight at 4°C. After washing with PBS-T (1 x DPBS with 0.1% Tween 20), organoids were cryoprotected in 30% sucrose solution until fully equilibrated. Samples were then embedded in gelatin solution (7.5% gelatin, 10% sucrose in 1xDPBS) at 37°C for 1 hour, snap-frozen in a dry ice/ethanol slurry, and stored at -80°C. Cryosectioning was performed to obtain 16-μm-thick sections. For immunofluorescence, sections were air-dried and outlined with a hydrophobic PAP pen before blocked with 5% normal goat serum in PBS-T for 1 hour, incubated overnight with primary antibodies (Supplementary Table 1) in primary antibody dilution buffer (PBS-T with 5% BSA and 0.05% sodium azide), and followed by secondary antibodies (Alexa Fluor® conjugates) for 1 hour at room temperature. Slides were washed, stained with DAPI solution (0.2 μg/mL), mounted with Antifade Mounting Medium (VECTASHIELD®, H-1000-10), and imaged at 10× magnification for whole organoid scans or 60× magnification for detailed cellular analysis using a fluorescence confocal microscope (Nikon Eclipse *Ti*) (Nikon, Tokyo, Japan) to assess neuronal organization of MLOs. The morphologies of neurons, astrocytes, and colocalization analysis were performed by taking multi-layer stacking (Z-stack) images under 60× oil immersion objective lens. Quantitative immunofluorescence analyses (e.g., cell counts for FOXP1+, FOXG1+, SOX2+ and Ki67+ cells, as well as marker colocalization) were performed using ImageJ (NIH) on at least 3 - 5 randomly selected non-overlapping fields of view (FOVs) per organoid section, with a minimum of 3 organoids per differentiation batch. Each FOV was imaged at consistent magnification (60x) and z-stack depth to

ensure comparable sampling across conditions. Data from individual FOVs were first averaged within each organoid to obtain an organoid-level mean, and then biological replicates (independent differentiations, n ≥ 3) were averaged to generate the final group mean ± SEM.

Genome editing patient iPSC clones

The iPSC line (GD2-1260) used for gene correction was derived from fibroblasts obtained from a GD Type 2 patient carrying compound heterozygous *GBA1* mutations (P415R/L444P) [29]. A guide (g) RNA was designed to target SpCas9-mediated double strand break introduction proximal to the L444P mutation (*GBA1* mutation at nt14446, T>C) in GD2-1260. Oligonucleotides (caccGAAGAACGA CCCGGACGCAG and aaacCTGCGTCCGGGTCGTTCTTC; overhangs in lower case; target mutation site underlined; IDT) transcribing the sgRNA target sequence were annealed and cloned via BbsI restriction digest into plasmid pX458M that contains a U6 promoter-driven sgRNA and a SpCas9-2A-EGFP expression cassette. The pX458M plasmid is modified from the pX458 plasmid (addgene #48138) [33] and carries an optimized sgRNA scaffold [34]. The targeting activity of this plasmid was validated by T7E1 assay using 293 cells. GD2-1260 cells were transfected with pX458M and a phosphorothioate-modified single stranded oligonucleotide (ssODN; IDT) donor template using TransIT-LT1 (Mirus). The ssODN (Supplementary Figure 1A) was designed to introduce the desired wildtype *GBA1* sequence flanked by homology arms to the targeted genomic region. The ssODN was also designed to contain silent mutations to prevent retargeting by SpCas9 and to introduce a BtgI restriction site to facilitate identification of targeted clones. Forty-eight hours post-transfection, GFP-positive cells were isolated by FACS and replated at cloning density (250-500 cells/well of a 6 well matrigel-coated plate). Replated cells were cultured for 4 days in mTeSR1 containing 10% CloneR (StemCell Technologies), using the manufacturer's recommended protocol. Cells were subsequently fed daily with mTeSR1 for an additional 9 days before colonies were manually harvested and expanded for genotyping. Primers VS4247 (gtgcgtaactttgtcgacagtcc) and VS4249 (ctgagagtgtgatcctgccaag) were used to PCR amplify the targeted *GBA1* genomic region and products were subjected to BtgI digestion to identify putative edited clones. Selected clones were subsequently confirmed by Sanger sequencing. This gene editing strategy is expected to also target the *GBA1* pseudogene due to the identical target sequence which limits the gene correction on certain mutations (e.g., P415R) [35,36], but the chance to target other off-targets is low due to low off-target scores ranked based on the MIT Specificity Score analysis [37].

SapC-DOPS-fGCase treatment of MLOs

As previously described [38,39], SapC-DOPS nanovesicles were formulated by combining saposin C (SapC) with dioleoylphosphatidylserine (DOPS) to encapsulate either recombinant human acid β-glucosidase (fGCase, Freeline Therapeutics) or fluorescent CellVue Maroon (CVM) for uptake studies. The SapC-DOPS-fGCase complex was prepared at a final concentration of 0.6 μg/mL fGCase and added to the BGM culture medium of MLOs derived from WT-75.1, GD2-1260, and GD2-10-257 hiPSC lines. To assess nanovesicle uptake, WT-75.1 MLOs at week 13 were co-cultured with SapC-DOPS-CVM for 48 hours, followed by confocal imaging to confirm internalization of the fluorescent CVM within the organoids.

For enzyme delivery and therapeutic evaluation, MLOs were treated with SapC-DOPS-fGCase or SapC-DOPS alone (control) for a 48-hour period to assess uptake and enzyme activity. For long-term treatment efficacy, MLOs were treated for two weeks before evaluating therapeutic efficacy. During treatment, MLOs were maintained in BGM media containing nanovesicles and were replaced every 3 days to ensure consistent exposure. Post-treatment, MLOs were harvested for confocal imaging, enzymatic assays, and biochemical analyses to assess GCase activity, protein expression, and correction of GD phenotypes.

AAV injection into MLOs

Transfer vector of AAV9-GBA1 virus containing GBA1/GFP expressing cassette (CB-GBA1-IRES-GFP) was packaged in AAV9 capsid at AAVnerGene (Rockville, MD, USA). For the delivery of AAV9-GBA1 gene therapy to MLOs, a precise injection protocol was employed using a nanoliter injector system

(World Precision Instruments). MLOs derived from WT-75.1, GD2-1260, and GD2-10-257 hiPSC lines were placed in a dish containing sterile 1 x PBS. A glass pipette connected to a gas injector was lowered into the center of each MLO at a desired depth of 200 to 300 μm, as determined by microscopic visualization. A volume of 500 nL (0.5μL) of AAV9-GBA1 vector, at a concentration of 3.6×10^{13} vg/mL, was injected into ten sites of MLOs at a volume of 50 nL per injection site. The injection glass needle was retracted slowly after completion of the injection to minimize damage and ensure vector distribution. Morphology and viability were assessed post-injection, and MLOs were then maintained in culture for 3 weeks prior to subsequent analyses.

Substrate Reduction Therapy treatment of MLOs

For evaluation of the tolerated dose of Substrate Reduction Therapy (SRT), WT-75.1 MLOs were treated with SRT compound GZ452 (AstaTech, P14969), also named GZ-682452, an analogue of venglustat [40], at concentrations of 0.3, 1, 2, and 3 μM starting on day 0 for a period of 6 weeks. MLO size was measured weekly using bright-field microscopy and analyzed with ImageJ software to assess morphological changes. For short-term SRT treatment, 13-week-old GD2-1260 MLO were treated with 300nM GZ452 for 3 weeks, with medium refreshed every 3 days to maintain consistent drug exposure. For long-term SRT treatment, GZ452 treatment at the concentration of 300nM was started at the beginning of MLO generation (day 1) and continued for 28 weeks before collection for analysis. Untreated MLOs served as controls.

Glycosphingolipids analyses

MLOs were washed with ice-cold PBS and homogenized and sonicated in sterile ddH_2O. Glycosphingolipids were then extracted from tissue homogenates using chloroform/methanol following protocol outlined previously [41]. Aliquots of lipids extracts were processed for GluCer and GluSph quantification by ultra-high-performance chromatography coupled to tandem mass spectrometry (UHPLC-MS/MS) using a Waters Xevo TQ-S Micro triple quadrupole mass spectrometer (Waters, Milford, MA) at CCHMC Clinical Mass Spectrometry Laboratory. Chromatographic separation for GluCer and GluSph was achieved using a XSelect CSH C18 XP Column (100 x 2.1 mm, 2.5 μm, Waters) column. Quantification by LC-MS/MS was operated in the multiple reaction monitoring (MRM) mode, with detection of the transition pair of the individual protonated parent ions of GluCers and daughter ion m/z 264.2. GluSph was measured by monitoring the mass transition m/z 462.3> 282.4. The sphingoid base for all GluCer species analyzed is d18:1. Calibration curves were prepared for C16 GluCer, C18 GluCer, C24 GluCer, and C24:1 GluCer using C18 glucosyl(ß) ceramide-D5 as the internal standard. Quantification of GluCer species with various fatty acid chain lengths was realized by the calibration curve of each species or with the closest fatty acyl chain length. The quantification of GluSph was based on the calibration curve using glucosyl(β) sphingosine-D5 as internal standard. The calibration curve for GluCer and GluSph was 25 pg–10 ng on column. Three QCs at low, medium and high levels (50 pg, 0.5 ng and 5.0 ng) were prepared in organic solvent and analyzed along with samples. The GluCer and GluSph levels in MLO were normalized to total MLO protein (mg) that were used for glycosphingolipids analyses. Protein mass was determined by BCA assay and glycosphingolipid was expressed as pmol/mg protein. Additionally, GluSph levels in the culture medium were quantified and normalized to the medium volume (pmol/mL) [42].

Measuring Dopamine levels by ELISA

Dopamine levels in MLO culture medium were quantified using the Dopamine ELISA Kit (Abnova) that involves dopamine extraction, acylation and enzymatic conversion before assay. Briefly, MLO culture medium was collected from 4 MLOs cultured in 3 mL BGM medium for 72 hours. Dopamine extraction was performed by pipetting 10 μL of standards, controls, and 750 μL of the sample into the extraction plate wells, filling each to 750 μL with deionized water, followed by 25 μL of TE buffer. Shake the covered plate for 60 minutes at room temperature (RT, 20-25°C) at 600 rpm, wash with 1 mL wash buffer twice, then acylate with 150 μL acylation buffer and 25 μL acylation reagent for 20 minutes. After washing again, elute with 100 μL hydrochloric acid, and

transfer 90 µL of supernatant to the microtiter plate for enzymatic conversion with 25 µL freshly prepared enzyme solution, incubating at 37°C for 2 hours. Then, 100 µL of the converted samples and 50 µL dopamine antiserum were added to the dopamine microtiter strips. The mixture was then incubated overnight at 2-8°C. The strips were then washed and incubated with 100 µL enzyme conjugate for 30 minutes, followed by 100 µL of substrate for 20-30 minutes, and finally, 100 µL of stop solution was added. Absorbance was measured at 450 nm within 10 minutes, and dopamine concentrations were calculated using a calibration curve, applying the correction factor (10/500 = 0.02) to adjust and normalize by sample volume.

GCase activity assay

GCase enzyme activities in hiPSCs and MLOs were determined fluorometrically with 4-methylumberlliferyl-β-D-glucopyranoside (4MU-Glc) in the presence of the GCase irreversible inhibitor, Conduritol B epoxide (CBE, 2 mM, Millipore, Bedford, MD) as previously described [43]. Briefly, hiPSC cell pellet or MLO tissues were homogenized using Precellys Evo Homogenizer/CK Mix beads (Bertin Technologies, France) in 1% sodium taurocholate/1%Triton X-100 (Tc/Tx) solution. GCase enzyme activity was then determined by 4MU-Glc as substrate in 0.25% Tc/Tx diluted in 0.1 M citrate phosphate buffer (pH 5.6). Protein concentrations were determined by BCA assay for normalization. The GCase-specific activity was calculated by subtracting non-specific activity (with CBE) from total activity (without CBE) and normalized to total protein mass.

Transcriptome analysis of MLOs

Total RNAs were extracted from week 8 MLOs using the RNeasy Mini Kit (Qiagen). Total RNAs (150 to 300 ng), quantified by Qubit (Invitrogen) high-sensitivity spectrofluorometric assay, were poly-A selected and reverse transcribed using Illumina's TruSeq® stranded mRNA library preparation kit (Illumina). Each sample was fitted with one of 96 adapters containing different 8-base molecular barcodes for high-level multiplexing. After 15 cycles of PCR amplification, completed libraries were sequenced on NovaSeq 6000 (Illumina), generating 30 million high-quality 100-base-long paired-end reads per sample. A quality control check on the fastq files was performed using FastQC. Upon passing basic quality metrics, the reads were trimmed to remove adapters and low-quality reads using default parameters in Trimmomatic (Version 0.33). The trimmed reads were then mapped to human reference genome GRCh38 using default parameters with strandness option in Hisat2 (Version 2.0.5), achieving a mapping rate greater than 90%. Transcript or gene abundance was determined using kallisto (Version 0.43.1). A transcriptome index in kallisto was created using Ensembl cDNA sequences for the reference genome. This index was then used to quantify transcript abundance in raw counts and transcript per million (TPM). Differential expression analysis was performed using the R package DESeq2 [44]. Genes with BaseMean ≥ 50, |fold change| ≥ 2, p-adj ≤ 0.05 were identified as differentially expressed genes (DEGs). Heatmaps were made using the R package ggplot2. Gene enrichment analysis using cellular component, KEGG pathways, molecular function, and biological process (GO analysis) was performed using DAVID 6.8 [45]. Three MLOs were pooled for each sample and three samples were profiled for each genotype. MLO Sequencing datasets and partially processed results have been deposited to the National Center for Biotechnology Information (NCBI)'s Gene Expression Omnibus (GEO) database (GSE303993).

Gene expression analysis by qRT-PCR

Total RNA was isolated from MLO tissue using the RNeasy Kit (Qiagen). Quantitative RT-PCR was carried out as described previously using primers listed in Supplementary Table 1 [46]. Housekeeping gene *GAPDH* or *ACTB* was used as internal controls for mRNA quantification. Relative expression of mRNAs was determined by the $2^{-\Delta\Delta}$CT method.

Immunoblotting

Immunoblotting was used to detect protein expression in iPSCs and MLOs. Briefly, brain organoids or cells were homogenized in freshly prepared RIPA buffer with protease inhibitors and anti-phosphatase inhibitors using a Precellys Evo Homogenizer (Bertin). The samples were then centrifuged at 12,000 *g* for 10 min to produce lysate for electrophoresis, membrane transferring, and detection using primary and secondary antibodies indicated in Supplementary Table 1. Semi-quantification of proteins was performed using ImageJ (NIH).

Statistical analysis

For comparisons between two groups, data were analyzed using unpaired two-tailed Student's t-tests when the sample size was ≥ 6 per group and normality was confirmed by the Shapiro-Wilk test. When the normality assumption was not met or when sample sizes were small (n < 6), the non-parametric Mann-Whitney U test was used instead. For comparisons involving three or more groups, one-way ANOVA followed by Tukey's multiple comparison test was applied when data were normally distributed; otherwise, the non-parametric Dunn's multiple comparison test was used. Exclusion of outliers was made based on cutoffs of the mean ±2 standard deviations. All statistical analyses were performed using GraphPad Prism 10 software. Exact p-values are reported throughout the manuscript and figures where feasible. A p-value < 0.05 was considered statistically significant.

Results

Generation and characterization of MLOs derived from hiPSCs

To generate MLOs from iPSCs, healthy hiPSCs were differentiated following a stepwise protocol, neural induction, neuroepithelial expansion, and maturation, adopted with modifications from previous studies [31,32] (Figure 1A). Midbrain specification during development requires appropriate posterior differentiation signals [47,48]. Our protocol used sequential activation/inhibition of critical signaling pathways involved in midbrain specification: Wnt signaling (activated by CHIR99021), BMP signaling (inhibited by dual-SMAD), and FGF signaling (activated by FGF8) (Figure 1A). MLOs were matured and characterized using immunofluorescence, gene expression, and immunoblotting. Week 8 MLOs showed diverse neural cell types, including pan-neurons (Tuj1/NeuN), astrocytes (GFAP), dopaminergic (DA) neurons (FOXA2/TH), and neural progenitor cells (SOX2/Ki67) (Figure 1B). Comparative analysis of forebrain marker FOXG1 expression between MLOs and cerebral organoids (COs) showed barely detectable FOXG1 in MLOs (Figure 1C). Quantitative RT-PCR analysis demonstrated a significant increase in midbrain/DA neuron-specific genes (*FOXA2*, *ASCL1*, *LMX1A*, *PLZF*, and *TH*) from week 3 and week 8 MLOs, demonstrating the midbrain identity of these organoids. Expression of glial-specific genes (*GLAST*, *S100B*) increased over time, while pluripotency markers (*SOX2*, *NANOG*, *OCT4*) were downregulated, suggesting progressive neural differentiation (Figure 1D). Immunoblot further validated hiPSCs differentiation into MLOs by expression of neuronal (Tuj1, MAP2), DA neuronal (TH), and glial (GFAP, S100B) markers at week 8, with reduced Sox2 expression in MLOs versus hiPSCs (Figure 1E). Together, these results confirm the successful generation of MLOs with midbrain-like cellular composition and molecular identities.

GCase deficiency in GD MLOs leads to glycosphingolipids accumulation and altered transcriptomic profiling

To model nGD and investigate the impact of GCase deficiency on MLOs, we generated GD MLO using the GD2-1260 hiPSC line derived from GD Type 2 patient harboring *GBA1*$^{L444P/P415R}$, compound heterozygous mutations, using same protocol in Figure 1 (Figure 2) [29]. Midbrain identity of GD MLOs was confirmed by TH/FOXA2 expression (Figure 3). Immunoblot showed an approximately 85% reduction in GCase protein levels in week 8 GD2-1260 MLOs versus WT-75.1 MLOs (Figure 2A). Consistent with reduced GCase protein, GCase activity decreased to 14.2% in

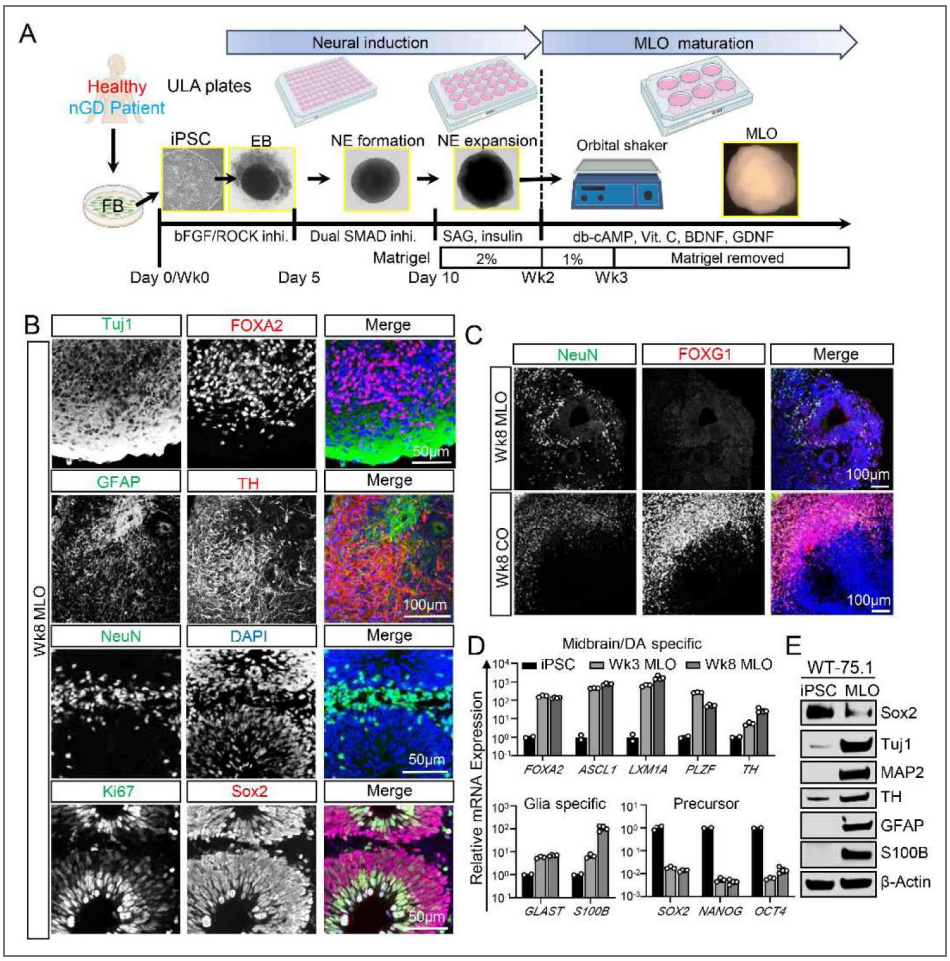

Figure 1. Generation and characterization of midbrain-like organoids (MLOs) from healthy human (h) iPSCs (WT-75.1 hiPSCs).

(A) A schematic overview of the procedures for generating MLOs from healthy WT-75.1 hiPSCs. (B) Representative confocal images showing architectural structure of week (Wk) 8 MLOs containing new-born neurons (Tuj1/NeuN), astrocytes (GFAP), dopaminergic neurons (FOXA2/TH) and neural progenitor cells (SOX2/Ki67). Merge images show the distribution of those cell markers. (C) FOXG1 expression in MLO and cerebral organoid (CO). Transcription factor FOXG1 (forebrain marker) was enriched in CO at Wk8 of differentiation but absent in MLO. Pan-neurons (NeuN) were both present in MLO and CO, as shown by NeuN immunostaining (neuronal marker). (D) Quantitative analysis of cell type specific genes expression for midbrain/dopaminergic neuron (*FOXA2*/*ASCL1*/*LXM1A*/*PLZF*/*TH*), glial cells (*GLAST*/*S100B*) and multipotent stem cells (*SOX2*/*NANOG*/*OCT4*) in Wk3 and Wk8 MLOs (n=3 MLOs pooled for each group) by qRT-PCR. (E) Immunoblot of Sox2, Tuj1, MAP2, TH, GFAP and S100B in WT-75.1 hiPSCs and its derived MLO (Wk8, n=3 MLOs pooled for each group) lysate. β-Actin was used as a loading control.

GD2-1260 hiPSCs and 15.0% in GD2-1260 MLOs vs. WT-75.1 ($p < 0.001$; Figure 2B). Bright-field imaging at weeks 4, 8, and 15 showed no difference on overall MLOs appearance between WT-75.1 and GD2-1260 MLOs (Figure 2C). MLO size measurements revealed a trend toward smaller GD2-1260 MLOs versus WT-75.1 at week 8, though not statistically significant (Figure 2D).

Loss of GCase function in GD disrupts glycosphingolipids metabolism, a primary pathogenic factor in nGD [49]. Mass spectrometry analysis demonstrated significant glycosphingolipid substrate accumulation in GD2-1260 MLOs. At week 15, total glucosylceramide (GluCer) level was elevated approximately 1.39-fold in GD2-1260 MLOs compared to WT-75.1 MLOs ($p < 0.05$; Figure 2E). GluCer analysis revealed marked accumulation of species 18:0 and 16:0, particularly brain predominant species (18:0) in GD2-1260 MLOs, while other species remained largely unchanged (Figure 2F, Supplementary Figure 2). Similarly, glucosylsphingosine (GluSph), a toxic lipid associated with nGD [4,40,50], was significantly elevated approximately 3.3-fold and 5.6-fold in GD2-1260 MLOs at weeks 15 and 28, respectively, versus WT-75.1 controls (Figure 2G, Supplementary Figure 2). These findings indicate profound lipid substrates dysregulation in GCase-deficient GD MLOs, consistent with the biochemical hallmark of GD.

To explore the transcriptomic consequences of GCase deficiency, we performed bulk RNA sequencing on week 8 MLOs, when DA neurons maturation and GD phenotypes were evident. Principal component analysis (PCA) revealed distinct clustering of WT-75.1 and GD2-1260 MLOs, with the first principal component accounting for 53% of the variance, indicating significant transcriptomic differences between two genotype groups (Figure 2H). An MA plot identified 1,429 differentially expressed genes (DEGs) in GD2-1260 MLOs compared to WT-75.1, with 664 genes upregulated and 765 genes downregulated. GO analysis of these DEGs revealed significant enrichment in pathways including cAMP, PI3K-AKT, and WNT signaling that control the nervous system development, axon guidance, and neuron differentiation (Figure 2J). KEGG analysis similarly identified dysregulation in neural signaling pathways, synaptic transmission, and lysosomal function (Figure 2K). The heatmap of these DEGs elucidated specific gene expression changes within key pathways (Figure 2L-2O), including WNT signaling (Figure 2L) [30], anterior-posterior brain specification (Figure 2M), neuronal function (Figure 2N), and lysosome-phagosome (Figure 2O) in GD2-1260 MLOs, with many genes exhibiting upregulation or downregulation consistent with nGD pathology.

Collectively, these results demonstrate that *GBA1* mutation in GD MLOs leads to reduced enzyme activity, causes lipid substrate accumulation, and alters transcriptomic profiles, particularly in neural development, signaling, and lysosomal function. These findings provide insights into nGD mechanism and support MLOs as a model for studying nGD.

Skewed specification of midbrain patterning and dopaminergic neuron differentiation in GD MLOs

Building on the molecular and transcriptomic hallmarks of GCase deficiency observed in nGD MLOs (Figure 2), we next investigated the impact on midbrain patterning and dopaminergic neuron differentiation (Figure 3). Firstly, RNA sequencing data revealed elevated FOXG1 and PAX6, and reduced FOXP1 mRNAs in GD2-1260 MLOs versus WT-75.1 MLOs at week 8 (Figure 2M, Figure 3A). These genes are fate-determining regulators in controlling proper anterior-posterior neural patterning [51–53]. Immunofluorescence confirmed reduced FOXP1+ and increased FOXG1+ cell counts in GD2-1260 MLOs (Figure 3B, 3C). About 11.6% cells were FOXP1+ FOXG1+ cells in GD2-1260 MLOs, but they were barely seen in WT-75.1 MLOs. These results indicate a significant disruption in expression of genes involved in forebrain and midbrain patterning in GD MLOs.

The skewed specification of midbrain patterning may contribute to dysregulated dopaminergic neuron development in GCase-deficient GD MLOs (Figure 3). There were clear differences in the expression of midbrain-specific markers between WT-75.1 and GD2-1260 organoids at week 6 (Figure 3D). In WT-75.1 MLOs, FOXA2 (a midbrain progenitor marker) and TH (dopaminergic neuron marker) were strongly expressed and co-localized (Figure 3D, 3E), indicating normal

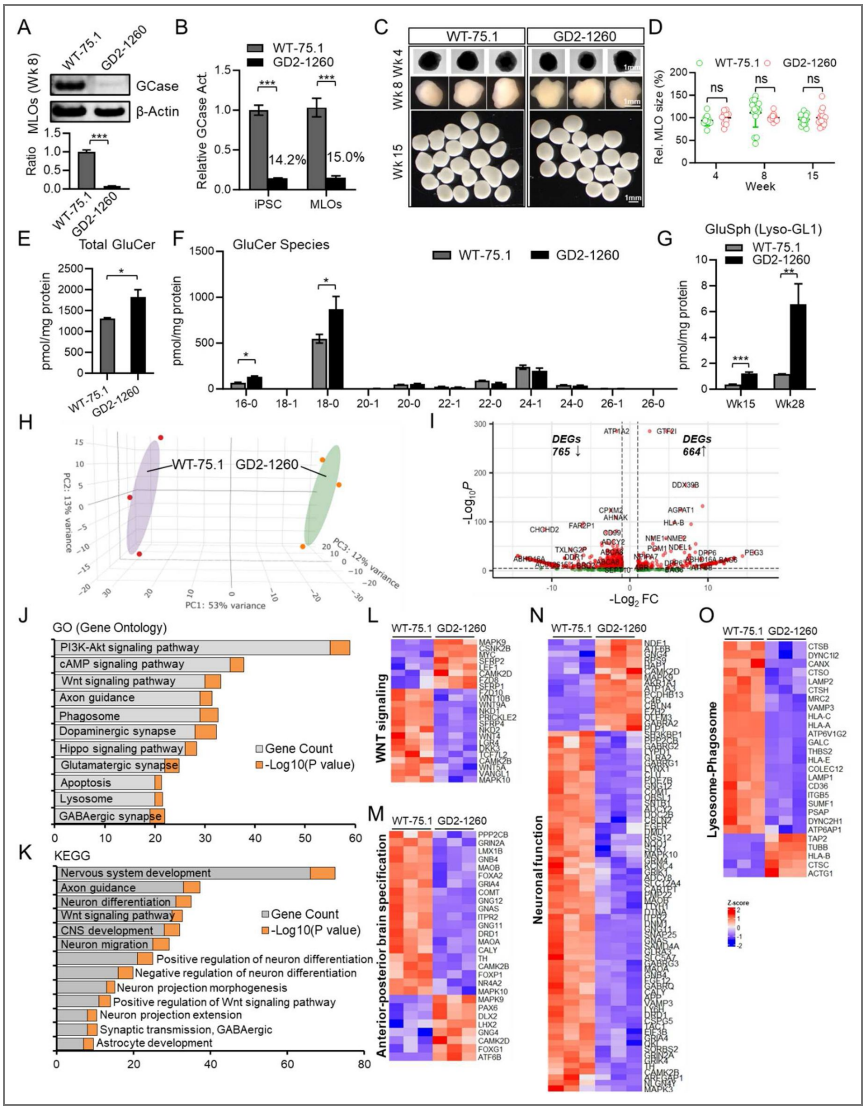

Figure 2. GCase deficiency drives glycosphingolipids accumulation and transcriptomic alteration in GD MLOs.

The GD MLOs were generated as in Figure 1A. (A) Reduced GCase protein in GD MLO (GD2-1260). Wk 8 MLOs (n=3) were pooled as a biological sample. β-Actin was used as loading control. (B) GCase activity in hiPSCs and MLOs (> 3 MLOs were pooled for each group). Data was normalized to WT-75.1 control. (C) Representative images of WT-75.1 and GD2-1260 MLOs at Wks 4, 8 and 15 of differentiation. (D) MLO size was measured based on area of MLO spheres and normalized to WT-75.1 control at each indicated time points. N ≥ 10 MLOs were quantified per group. (E, F) Measurement of total glucosylceramide (GluCer) and GluCer species in Wk 15 MLO. (B, D, E. G) *p < 0.05, ***p < 0.001, ns, not significant, unpaired Student's t test. (G) Glucosylsphingosine (GluSph) levels in Wk15 and Wk28 MLOs (3~5 MLOs were pooled for each group). GluCer and GluSph levels in the organoids were measured by LC-MS/MS and normalized by corresponding total protein of MLO tissue lysate. (H) 3D Principal Component Analysis (PCA) of bulk RNA sequencing (RNA-seq) data. The Euclidean distance of the normalized gene expression among healthy control (WT-75.1) and GD (GD2-1260) MLOs was used for sample clustering. Ellipsoids around each group indicate the distribution and spread of the samples within the sample group. Wk 8 MLOs (n=3) were pooled as one biological sample, and three samples were profiled in each group. (I) MA plot showing the distinct genes differentially expressed in GD MLOs. Statistically significant differentially expressed genes (DEGs; |fold change|≥ 1, p-adj ≤ 0.05 and base mean ≥ 50) were highlighted in red. Number of DEGs downregulated and upregulated in GD2-1260 MLO against WT-75.1 MLO were shown. FC, fold-change. (J, K) Dysregulated pathway in GD MLOs analyzed by GO (gene ontology) (J) and Kyoto Encyclopedia of Genes and Genomes (KEGG) (K) enrichment of DEGs. Both gene counts and level of significance (-log10 of *p* value) were shown as stacked columns for each category. (L-O) Heat maps of dysregulated pathways or biological functions in GD MLO. Specifically, aberrant expressions of genes involved in WNT signaling (L), anterior-posterior brain specification (M), neuronal function (N) and lysosome-phagosome (O) were shown.

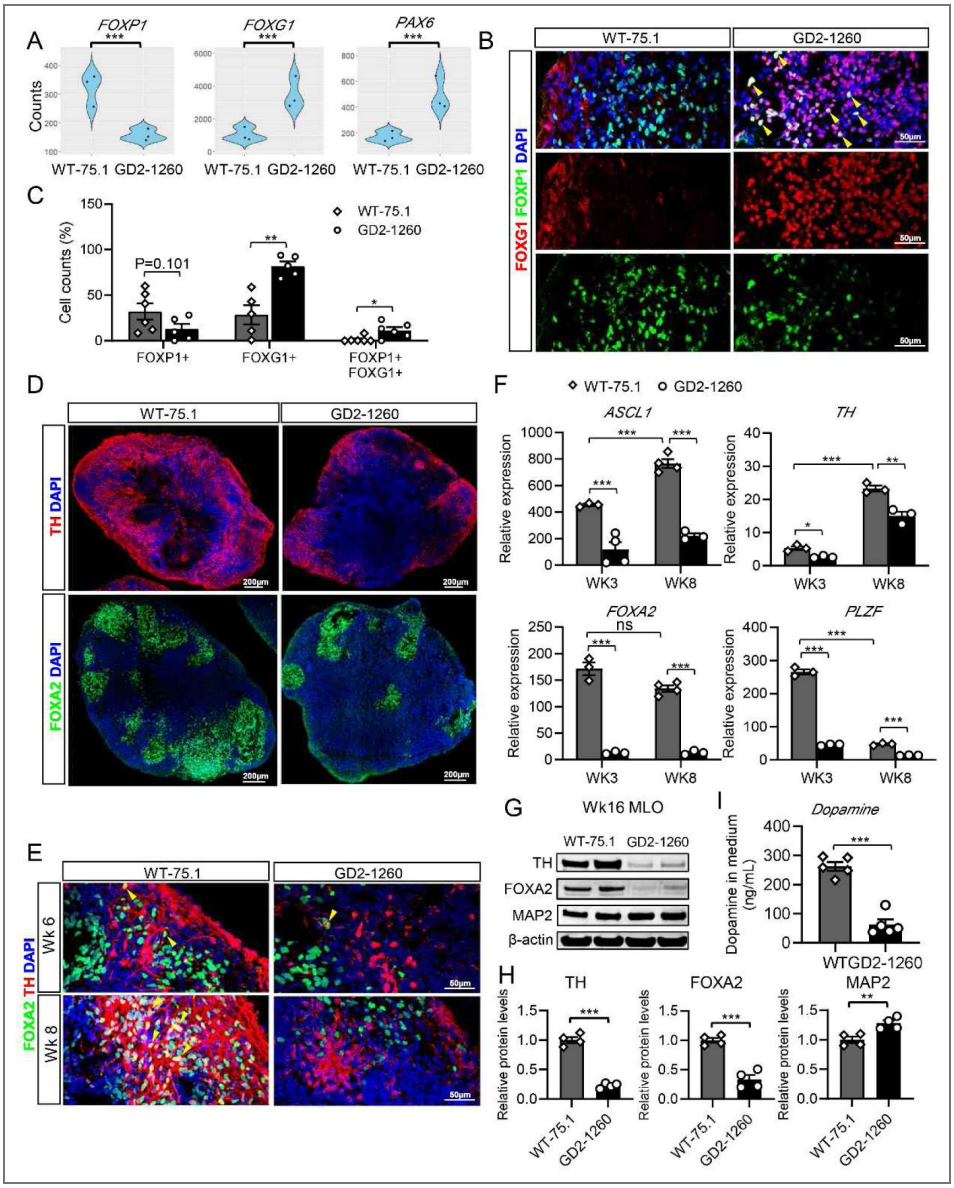

Figure 3. Skewed specification of midbrain patterning and dopaminergic neuron differentiation in GD MLOs.

(A) Gene expression of *FOXP1*, *FOXG1*, and *PAX6* in week 8 WT-75.1 and GD2-1260 MLOs. Data were plotted using RNA sequencing counts. ***p < 0.001, unpaired Student's t test. (B, C) Aberrant expression of FOXP1/FOXG1 transcription machinery for forebrain/midbrain patterning in GD MLOs. Representative confocal images (B) and quantification of Wk8 WT-75.1 and GD2-1260 MLOs, immunostained for FOXP1 (red) and FOXG1 (green), with DAPI (blue) labeling nuclei. Yellow arrows indicate FOXP1+FOXG1+ cells. Scale bar, 50 μm. *p < 0.05, **p < 0.01, unpaired Student's t test. (D) Confocal images of Wk6 MLOs, immunostained for midbrain patterning markers FOXA2 (green) or TH (red), with DAPI (blue) labeling nuclei. Scale bar, 100 μm. (E) Representative images of differentiating DA neurons in MLOs derived from WT-75.1 and GD2-1260 hiPSCs. TH (red), FOXA2 (green) were co-stained, with DAPI (blue) labeling nuclei. Yellow arrows indicate TH+FOXA2+ cells. Scale bar, 50 μm. (F) Quantification of midbrain progenitor markers *ASCL1*, *TH*, *LMX1A*, and *PLZF* expression in WT-75.1 and GD2-1260 MLOs at Wk3 and Wk8, measured by qRT-PCR and normalized to WT-75.1 hiPSC cells. Data are presented as mean ± SEM (n = 3-4 MLOs per group). *p < 0.05, **p < 0.01. (G) Immunoblot analysis of midbrain/dopaminergic neuron markers TH, FOXA2, and MAP2 in Wk16 MLOs. Protein samples were extracted from n=3 MLOs from each group. β-Actin was used as a loading control. (H) Relative protein levels of TH, FOXA2, and MAP2 in Wk8 GD2-1260 MLOs compared to WT-75.1. *p < 0.05, **p < 0.01, unpaired Student's t test. (I) Dopamine levels in MLO culture medium assay by ELISA. Culture medium from 4 GD2-1260 MLOs or WT-75.1 MLOs at Wk12 cultured in 3 mL BGM medium for 72 hours was assayed. Data are presented as mean ± SEM (n = 5 per group). ***p < 0.001, unpaired Student's t test.

midbrain patterning. In contrast, GD2-1260 MLOs showed markedly reduced FOXA2+, TH+ and FOXA2+TH+ cells (Figure 3D, 3E). Quantitative analysis confirmed the significant reduction of midbrain progenitor markers (*ASCL1*, *TH*, *FOXA2*, and *PLZF*) in GD2-1260 MLOs versus WT-75.1 (Figure 3F). At week 8, expression levels of *ASCL1*, *TH*, *FOXA2*, and *PLZF* were significantly reduced by approximately 71.0%, 44.4%, 90.0% and 69.8%, respectively, indicating a profound impairment in midbrain progenitor specification due to GCase deficiency. Immunoblot showed ~77.5% and ~66.5% reductions in TH and FOXA2, respectively, and a 27.7% increase in MAP2 in GD2-1260 versus WT-75.1 MLOs (Figure 3H). Dopaminergic function was determined by measuring dopamine levels in the culture medium (Figure 3I). Dopamine levels in week 12 MLOs culture medium (72 hours culture) were 76.0% ($p < 0.001$) lower in GD2-1260 MLOs versus WT-75.1 MLOs, confirming impaired dopaminergic function in GD MLOs.

These results indicate that GCase deficiency leads to skewed midbrain patterning and dopaminergic neuron differentiation, underscoring the critical role of GCase in midbrain development, as revealed for the first time, using patient iPSC-derived brain organoids.

CRISPR/Cas9-mediated *GBA1* mutation correction rescues disease phenotypes in GD MLOs

GD is an autosomal recessive disorder. Individuals who are carriers or heterozygous for *GBA1* mutations typically do not exhibit disease phenotypes [1]. To determine whether correction of the *GBA1* mutation could rescue GD phenotypes in GD MLOs, we used CRISPR/Cas9 technology to correct the L444P mutation in GD2-1260 hiPSCs ($GBA1^{L444P/P415R}$) and generated isogenic iso-GD2-1260 hiPSCs with a heterozygous genotype of $GBA1^{WT/P415R}$ (Figure 4A; Supplementary Figure 1). Karyotype analysis of GD2-1260 and iso-GD2-1260 demonstrated no detectable chromosomal abnormalities, confirming the genetic stability of both cell lines (Supplementary Figure 1D). Furthermore, genetic correction did not alter the expression of hiPSC related pluripotent genes (Supplementary Figure 1E). The MLOs derived from WT-75.1, GD2-1260, and iso-GD2-1260 hiPSCs were then compared to evaluating the impact of mutation correction on GD phenotypes.

At week 8, GCase protein in iso-GD2-1260 MLOs was restored to 45.8% of WT-75.1 levels (Figure 4B, 4C), consistent with correction of one *GBA1* allele [29]. GCase activity also improved, reaching 43.9% and 46.4% of WT-75.1 levels in GD2-1260 hiPSCs and MLOs, respectively, versus approximate 15% in GD2-1260 hiPSCs and MLOs (Figure 4D). Despite reduced GCase, early neural rosette formation in GD2-1260 MLOs remained largely unaffected in GD2-1260 and iso-GD2-1260, with similar counts of SOX2+Ki67+ proliferating neural progenitor cells in neural rosettes (Supplementary Figure 3A, 3B), suggesting early neural development is not impacted by *GBA1* L444P mutation.

GBA1 L444P mutation correction ameliorated lipid substrate accumulation in iso-GD2-1260 MLOs. GluSph levels which were elevated in GD2-1260 MLOs at weeks 15 and 28 (approximately 3.3-fold and 5.6-fold higher than WT-75.1, respectively; $p < 0.01$) was normalized to WT-75.1 levels (Figure 4E). Organoid size of iso-GD2-1260 MLOs was similar to WT-75.1 and GD2-1260 MLOs at week 4, 8 and 15 (Figure 4F, 4G).

Correction of the L444P mutation restored midbrain and dopaminergic neuron differentiation. TH and FOXA2 levels, which were reduced in week 16 GD2-1260 MLOs by approximately 76.4% and 72.4%, respectively, were restored in iso-GD2-1260 MLOs to WT-75.1 levels for TH, and approximately 53% of WT-75.1 levels for FOXA2 (Figure 4H, 4I). Dopamine levels in iso-GD2-1260 MLOs culture matched those in WT-75.1, unlike the reduced levels in GD2-1260 MLOs (Figure 4J), indicating restored dopaminergic function. The autophagy-lysosomal pathway, which is dysregulated in nGD, was partially corrected by *GBA1* mutation restoration (Figure 4K, 4L). Immunoblot analysis of lysosomal proteins showed that LAMP1 levels, which were significantly decreased in GD2-1260 MLOs by approximately 42.5% versus WT-75.1, were partially restored in iso-GD2-1260 MLOs (Figure 4K, 4L), however, Cathepsin D levels remained unchanged (Figure 4K, 4L). Dysregulated autophagy flux demonstrated by the elevated LC3-II and LC3-I was not significantly improved in isogenic MLOs compared to GD2-1260 MLOs (Figure 4M, 4N).

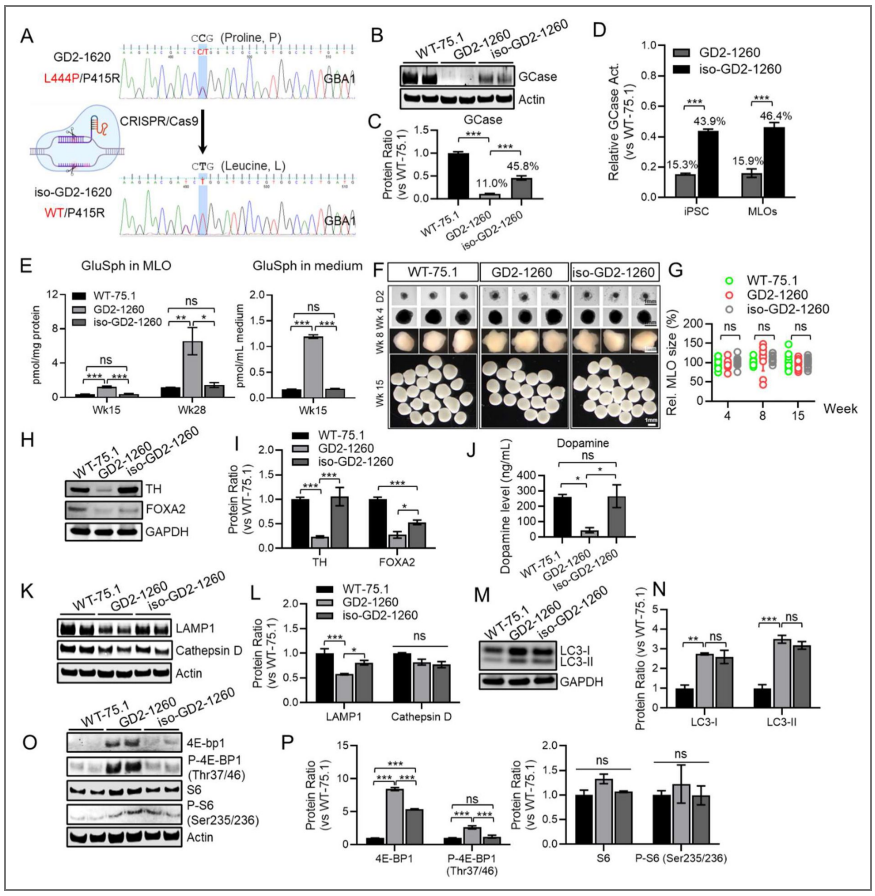

Figure 4. Mutation correction significantly rescued disease phenotypes in GD MLOs.

(A) Schematic overview of CRISPR/Cas9-mediated mutation correction of the *GBA1* L444P mutation in GD2-1260 hiPSCs, converting the L444P (L444P/P415R) mutation (Proline, P to Leucine, L) to the wild-type sequence (WT-P415R), generating isogenic iso-GD2-1260 hiPSCs. The mutated base C in amino acid code 'CCG' for proline (P), was corrected to T to decode leucine (L, CTG), which was confirmed by genome sequencing of *GBA1* locus. (B, C) Immunoblot analysis of GCase protein and quantification in week 8 MLOs derived from WT-75.1, GD2-1260, and iso-GD2-1260 hiPSCs. β-Actin was used as a loading control. Data are presented as mean ± SEM (n = 2 pooled, and 3 biological replicates per group). ***p < 0.001. (D) Relative GCase activity in GD2-1260 and iso-GD2-1260 hiPSCs and Wk8 MLOs, normalized to WT-75.1 controls. Data are presented as mean ± SEM (2 MLOs pooled, n = 3 per group). ***p < 0.001. (E) Measurement of GluSph levels in WT-75.1, GD2-1260, and iso-GD2-1260 MLOs at Wk15 and Wk28 and their culture medium at Wk 15, quantified by LC-MS/MS and normalized to total protein of tissue lysate. Data are presented as mean ± SEM. For GluSph in MLO, three MLOs were pooled and n = 3 per group. For MLO secreted GluSph, MLO culture medium in wells containing four MLOs were collected, n = 3 per group. **p < 0.01; ns, not significant. (F) Representative bright-field images of WT-75.1, GD2-1260 and iso-GD2-1260 MLOs at Day 2, Wks 4, 8, and 15 of differentiation. Scale bar, 1 mm. For side-by-side comparison, images for WT-75.1 and GD2-1260 at Wks 4, 8 and 15 were taken from Fig 2C. (G) MLO size quantification for WT-75.1, GD2-1260 and iso-GD2-1260 MLOs at Wks 4, 8, and 15. MLOs size was analyzed by NIS elements and presented as the area (μm^2) of MLO at indicated time point. N ≥ 10 MLOs were quantified per group. Data are presented as mean ± SEM. One-Way ANOVA, ns, not significant. (H, I) Immunoblot analysis of midbrain/dopaminergic neuron markers TH and FOXA2 (H) and their relative quantification (I) in Wk8 MLOs. Protein samples were extracted from n=3 MLOs from each group. GAPDH was used as a loading control. (J) Dopamine levels in the culture medium of Wk12 MLOs derived from WT-75.1, GD2-1260 and iso-GD2-1260 hiPSCs, measured after 72 hours in BGM medium (n = 4 MLOs per samples, 3 biological replicates). Data are presented as mean ± SEM (n = 5 per group). *p < 0.05, unpaired Student's t test. (K, L) Immunoblot analysis of autophagy-lysosomal pathway markers LAMP1 and Cathepsin D (K) and quantification (L) in Wk16 MLOs. GAPDH was used as a loading control. Data are presented as mean ± SEM. (M, N) Immunoblot analysis of LC3-I and LC3-II (M) and quantification (N) in Wk16 MLOs. Protein samples were extracted from n=3 MLOs for each group. GAPDH was used as a loading control. (O) Immunoblot analysis of mTOR signaling pathway components [4E-BP1, P-4E-BP1(THR37/46), S6, and P-S6 (Ser235/236)] in Wk16 MLOs. β-Actin was used as a loading control. (P) Quantification of protein levels of mTOR signaling pathway components. Data are normalized to WT-75.1 and presented as mean ± SEM. Immunoblot analysis for panel H and I and K-P was performed using the lysate from 3 MLOs pooled per group, 3 repeated experiments. ***p < 0.001; ns, not significant. One-way ANOVA test with Tukey's test.

GCase deficiency leads to mTOR hyperactivation in nGD [13,54,55]. In GD2-1260 MLOs, levels of 4E-BP1 and its phosphorylated form P-4E-BP1 (Thr37/46) were significantly elevated (Figure 4O). These levels were normalized or significantly reduced in iso-GD2-1260 MLOs. While S6 and its phosphorylated form (P-Ser235/236) remain unchanged (Figure 4O, 4P).

These results demonstrate that CRISPR/Cas9-mediated correction of *GBA1* mutation in GD2-1260 hiPSCs effectively rescues key nGD phenotypes and downstream effects, highlighting gene correction as a therapeutic strategy and validating MLOs as a preclinical disease model.

SapC-DOPS nanoparticle-mediated GCase enzyme therapy corrects GD phenotypes in GD MLOs

SapC-DOPS nanoparticles, composed of saposin C (SapC) and dioleoylphosphatidylserine (DOPS), showed promise as a CNS-targeted delivery system for lysosomal disorders like nGD [38,39]. The effectiveness of this approach in rescuing GD phenotypes was evaluated in MLOs derived from GD2-1260 hiPSCs and another GD2 hiPSC line, GD2-10-257, which carries the *GBA1*$^{L444P/RecNcil}$ mutation [56]. MLOs were derived from these hiPSCs following the protocol in Figure 1 and described in the Methods section. SapC-DOPS nanoparticle was formulated with a fGCase, a recombinant GCase variant with over 21-fold longer active half-life at lysosomal pH than wild-type GCase [57,58] (Figure 5A).

To test SapC-DOPS uptake, WT-75.1 MLOs were co-cultured with CVM (CellVue Maroon) loaded SapC-DOPS nanoparticles for 48 hours. CVM signals were detected throughout the organoids, confirming successful cargo delivery (Figure 5B). SapC-DOPS-fGCase was then prepared with 0.6 μg/mL fGCase [38] and cocultured with MLOs. After 48 hours, treatment significantly increased GCase activity in GD2-1260 MLOs, restoring it to approximately 66.7% of WT-75.1 levels, confirming efficient delivery (Figure 5C).

To evaluate efficacy, GD2-1260 and GD2-10-257 MLOs were treated for two weeks with SapC-DOPS or SapC-DOPS-fGCase. Confocal imaging confirmed restored GCase expression, with SapC-DOPS-fGCase-treated GD2-1260 and GD2-10-257 MLOs showing increased GCase approaching the level in WT-75.1 MLO (Figure 5D). Additionally, SapC-DOPS-fGCase treatment significantly elevated GCase load in both dopaminergic neurons (TH+) and astrocytes (GFAP+), as shown by colocalization of GCase with TH and GFAP in GD2-1260 and GD2-10-257 MLOs, respectively (Supplementary Figure 4A-D). Consistent with the results obtained with GD2-1260 MLOs (Figure 4H), reduction of TH in GD2-10-257 MLOs at weeks 16 and 28 were evident (Supplementary Figure 4E). Corresponding to increased GCase protein, SapC-DOPS-fGCase treatment elevated GCase activity to 2.3-fold of untreated WT-75.1 MLO (Figure 5E). In GD2-1260 MLOs, SapC-DOPS-fGCase fully restored GCase activity to WT levels, while SapC-DOPS alone had no effect (Figure 5F). Similar GCase restoration was observed in the additional patient organoids, GD2-10-257 MLOs, indicating the effectiveness of this approach across different GD MLO models with various *GBA1* mutations (Figure 5G). Importantly, SapC-DOPS-fGCase significantly reduced elevated GluSph levels in GD2-1260 and GD2-10-257 MLOs, matching WT-75.1 levels (Figure 5H, 5I), confirming effective lipid substrate clearance by delivered fGCase.

Furthermore, we evaluated the impact of SapC-DOPS-fGCase on the autophagy and lysosomal pathway and mTOR signaling. fGCase was found effectively delivered to lysosomal compartments, evidenced by colocalization of LAMP1 and LC3-II in treated GD2-1260 and GD2-10-257 MLOs (Supplementary Figure 5A-D), indicating restoration of GCase in lysosomal and autophagosome compartments. However, analysis of protein levels showed that decreased LAMP1 expression in GD2-1260 MLOs was not altered following SapC-DOPS-fGCase treatment (Figure 5J). The elevated LC3-II levels, an indicator of impaired autophagic flux, were reduced upon treatment, suggesting enhanced autophagic activity (Figure 5J). Moreover, phosphorylated 4E-BP1 (Thr37/46), but not total 4E-BP1, was improved in SapC-DOPS-fGCase treated MLOs, reflecting a decrease in mTOR hyperactivation (Figure 5J). We anticipate that a longer duration of SapC-DOPS-fGCase exposure in nGD MLOs may produce a more robust therapeutic effect in rescuing nGD-associated phenotypes, which will be evaluated in future studies.

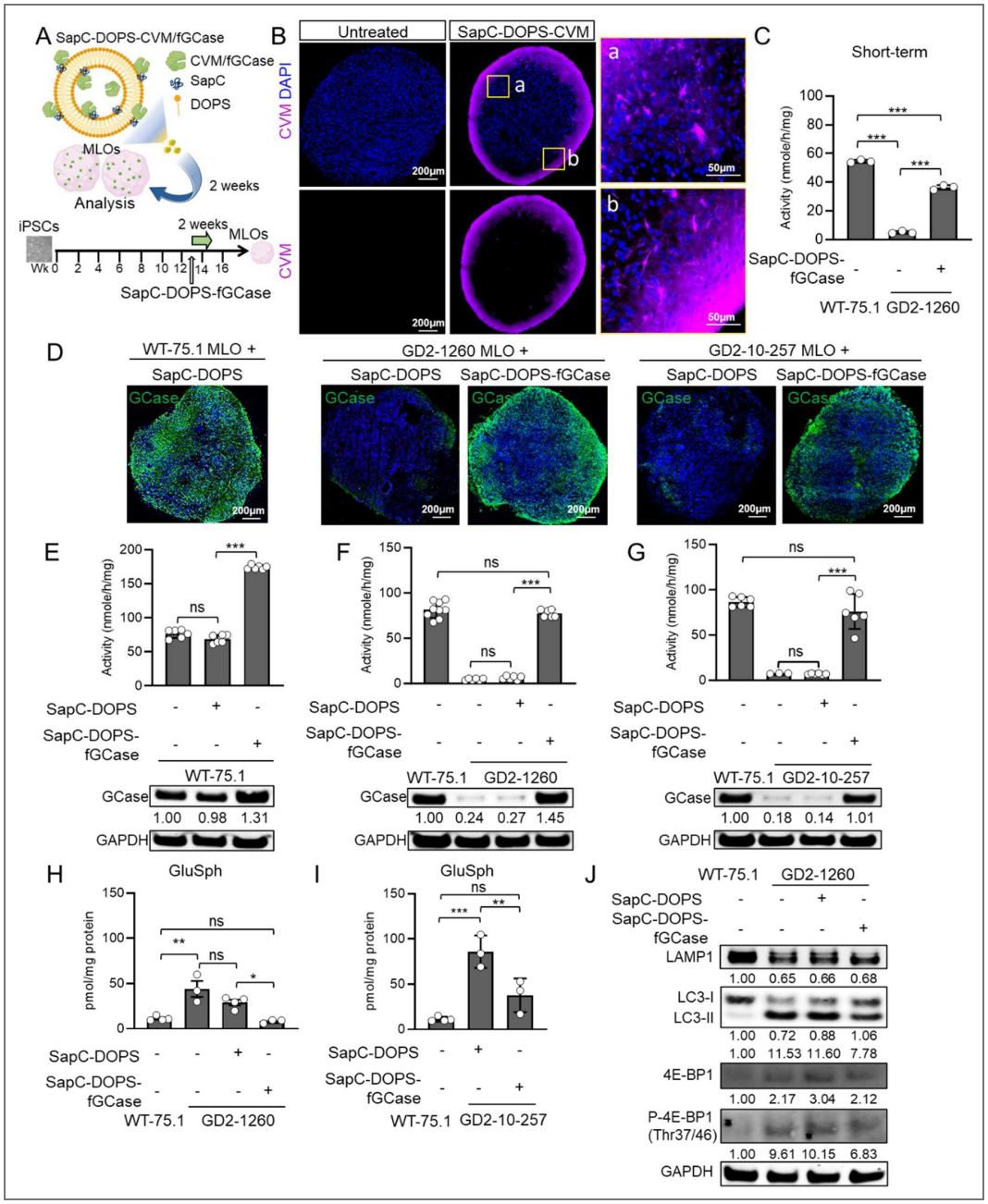

Figure 5. Delivery of GCase to MLOs via SapC-DOPS nanoparticles corrects GD phenotypes.

(A) Schematic illustration of SapC-DOPS nanoparticle-mediated delivery of recombinant GCase (fGCase) to MLOs. SapC-DOPS nanoparticles carrying fGCase or fluorescent label CVM were cocultured with MLOs, followed by short-term (48 hours) or 2-week treatment period before analysis. (B) Confocal images of untreated and SapC-DOPS-CVM-treated MLOs, showing uptake of CVM (magenta) with DAPI (blue) labeling nuclei. Scale bars: 200 μm (left panel), 50 μm (right panels, magnified regions a and b). (C) GCase activity in WT-75.1 and GD2-1260 MLOs following a 48-hour treatment with SapC-DOPS-fGCase. Data are presented as mean ± SEM (3 MLOs pooled, n = 3 per group). ***p < 0.001. (D) Confocal images of WT-75.1, GD2-1260, and GD2-10-257 MLOs treated with SapC-DOPS or SapC-DOPS-fGCase for 2 weeks, immunostained for GCase (green) with DAPI (blue) labeling nuclei. Scale bar, 200 μm. (E-G) GCase activity and protein in WT-75.1 and GD (GD2-1260, GD2-10-257) MLOs treated with SapC-DOPS or SapC-DOPS-fGCase for 2 weeks, measured by enzymatic assay and immunoblot. Data are presented as mean ± SEM (3 MLOs pooled, n = 3~4 per group). ***p < 0.001; ns, not significant. Protein samples were extracted from n=3 MLOs for each group. (H, I) GluSph levels in WT-75.1 and GD (GD2-1260, GD2-10-257) MLOs treated with SapC-DOPS or SapC-DOPS-fGCase for 2 weeks, quantified by LC-MS/MS and normalized to total protein. Data are presented as mean ± SEM (3 MLOs pooled, n = 3-4 per group). ***p < 0.001; **p < 0.01; ns, not significant. (J) Immunoblot analysis of autophagy-lysosomal and mTOR pathway proteins in SapC-DOPS or SapC-DOPS-fGCase treated GD2-1260 MLOs. GAPDH was used as a loading control. Protein samples were extracted from n=3 MLOs for each group. Protein levels are normalized to WT-75.1 untreated controls (set to 1.0).

In conclusion, the effective restoration of GCase activity and correction of selected molecular and biochemical GD phenotypes highlight both the utility of the MLO platform for studying nGD and the therapeutic potential of this nanoparticle-based approach for treating nGD.

AAV-mediated gene transfer in GD MLOs enhances GCase activity and mitigates GD phenotypes

AAV-based gene therapies have shown clinical safety and efficacy in neurodegenerative diseases [59,60]. Trials for GD Type 1 (NCT05487599) and Type 2 (NCT04411654) using AAV9 have initiated. While animal models support AAV's effectiveness in GD, its cellular impact on human or patient derived models remains unknown. To investigate the therapeutic effect of AAV gene therapy in human GD organoids, AAV9-GBA1 was injected at dose of 1.8×10^{10} vg per organoid at week 13 and evaluated 3 weeks after the injection (Figure 6A). In WT-75.1 MLOs, GCase activity was significantly increased in AAV9-GBA1-treated MLOs compared to untreated controls at week 15 (Figure 6B, left panel), suggesting effective transgene expression in normal organoids. AAV9-GBA1 restored GCase activity in GD2-1260 and GD2-10-257 MLOs to 47.8% and 37.7% of WT-75.1 levels, respectively ($p < 0.001$), compared to 6.0% and 8.8% in untreated controls (Figure 6B, middle and right panel). Immunoblot results further confirmed the restoration of GCase protein in AAV9-GBA1 treated GD MLOs (Figure 6B, bottom panel). Mass spectrometry analysis showed that AAV9-GBA1 normalized GluSph levels in GD2-1260 and GD2-10-257 MLOs, contrasting with elevated levels in untreated MLOs versus WT-75.1 controls (Figure 6C), indicating effective clearance of toxic lipid substrates in MLO by AAV gene therapy. Of note, LAMP1 levels were elevated after AAV9-GBA1 treatment, reflecting correction of lysosomal dysfunction (Figure 6D). However, the protein level of DA neuron marker (TH) was not significantly increased after AAV gene therapy compared to untreated group, suggesting longer treatment or earlier gene therapy intervention might be needed to recover dopaminergic neurons. Confocal imaging corroborated that AAV9-GBA1-treated GD2-1260 MLOs exhibited GFP signals and restored GCase expression in pan-neurons, DA neurons and astrocytes (Figure 6E).

These results collectively demonstrate that AAV9-GBA1 gene therapy effectively corrected GCase deficiency, reduced GluSph accumulation, and ameliorates lysosomal pathology in GD MLOs, highlighting its therapeutic potential for nGD.

Substrate Reduction Therapy reduces lipid accumulation and improves lysosomal function in GD MLOs

Current Substrate Reduction Therapy (SRT) in the standard clinical treatments for GD [61,62] has limited efficacy in addressing the neurological manifestations of nGD due to their inability to cross the blood-brain barrier efficiently. GZ-682452 (termed herein as GZ452) is an analogue of venglustat that is presently under clinical evaluation for treating nGD [63]. To evaluate the human MLO as a preclinical model for SRT drug development, we assessed GZ452's effects on MLO growth, lipid accumulation, midbrain markers, and lysosomal function.

GZ452 toxicity was first evaluated in WT-75.1 MLOs. Treatment at 0.3, 1, 2, 3 μM over 6 weeks modestly reduced MLO size at 1 μM, with the 2 μM and 3 μM doses significantly decreasing size versus untreated controls (Figure 7A), indicating high dose of GZ452 notably suppressed MLO growth. We next tested GZ452 at doses (0.01, 0.05, 0.3 μM) over 6 weeks in WT-75.1 MLOs. GZ452 dose-dependently reduced total GluCer levels (Figure 7B) and GluCer species, with the 0.3 μM dose showing the most pronounced effect (Figure 7C).

Expression of midbrain markers *ASCL1*, *TH*, and *PLZF* in WT-75.1 MLOs was largely unaffected by GZ452 (0.3 μM) treatment started at week 6, with no significant changes in relative mRNA levels compared to untreated controls (Supplementary Figure 6). We therefore applied this optimal tolerated GZ452 dose of 0.3 μM (300nM) in short-term (2 weeks) and long-term (up to 28 weeks) treatment to test its therapeutic effects in GD MLOs. After two weeks of treatment starting in week 13, GZ452 significantly ameliorated GluCer and GluSph accumulation in GD2-1260 MLOs (Figure 7E, 7F). Long-term GZ452 treatment from day 2 to week 28 robustly cleared GluSph storage

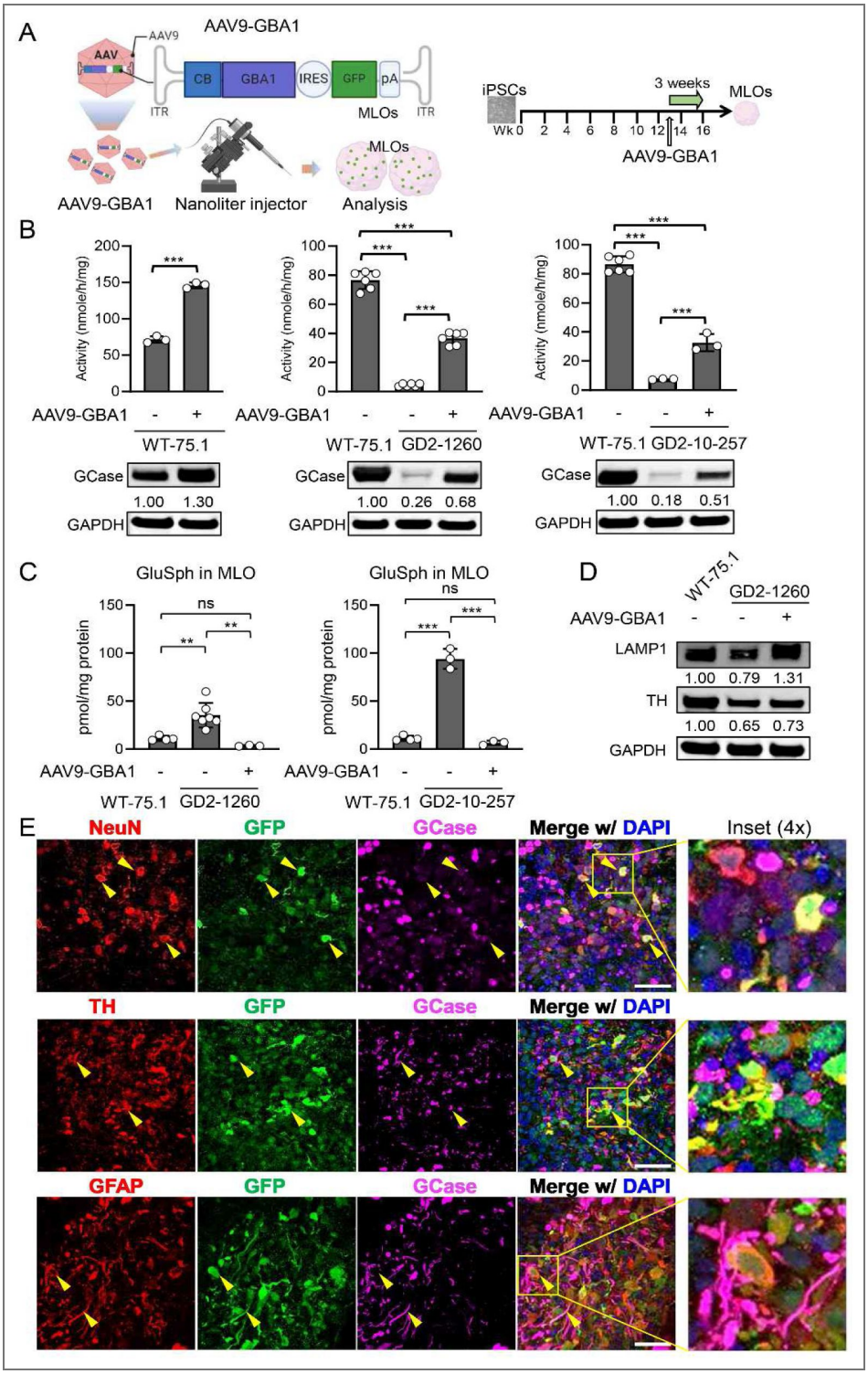

Figure 6. AAV9-GBA1 gene therapy mitigates disease phenotypes in GD MLOs.

(A) Schematic illustration of AAV9-*GBA1* gene therapy delivery to MLOs using a nanoliter injector. AAV9 vectors carrying the GBA1 gene (AAV9-GBA1) are administered to Wk13 MLOs. The samples were analyzed after 3 weeks of treatment. (B) GCase activity in WT-75.1, GD2-1260, and GD2-10-257 MLOs and AAV9-GBA1 treated MLOs were measured by enzymatic assay. Data are presented as mean ± SEM (3 MLOs pooled, n = 3 to 6 per group). ***p < 0.001. (C) GluSph levels in AAV9-GBA1 treated GD and control MLOs were quantified by LC-MS/MS and normalized to total protein. Data are presented as mean ± SEM (3 MLOs pooled, n ≥ 3 per group). ***p < 0.001; ns, not significant. (D) Immunoblot analysis of LAMP1 and TH in WT-75.1 and in GD2-1260 MLOs untreated or treated with AAV9-GBA1. Protein samples were extracted from n=3 MLOs for each group. Protein levels are normalized to WT-75.1 untreated controls (set to 1.0). (E) Transgene expressions (yellow arrows and enlarged insert) in neurons (NeuN), DA neurons (TH) and astrocytes (GFAP) of AAV9-GBA1 treated GD2-1260 MLOs. Scale bar = 50 μm.

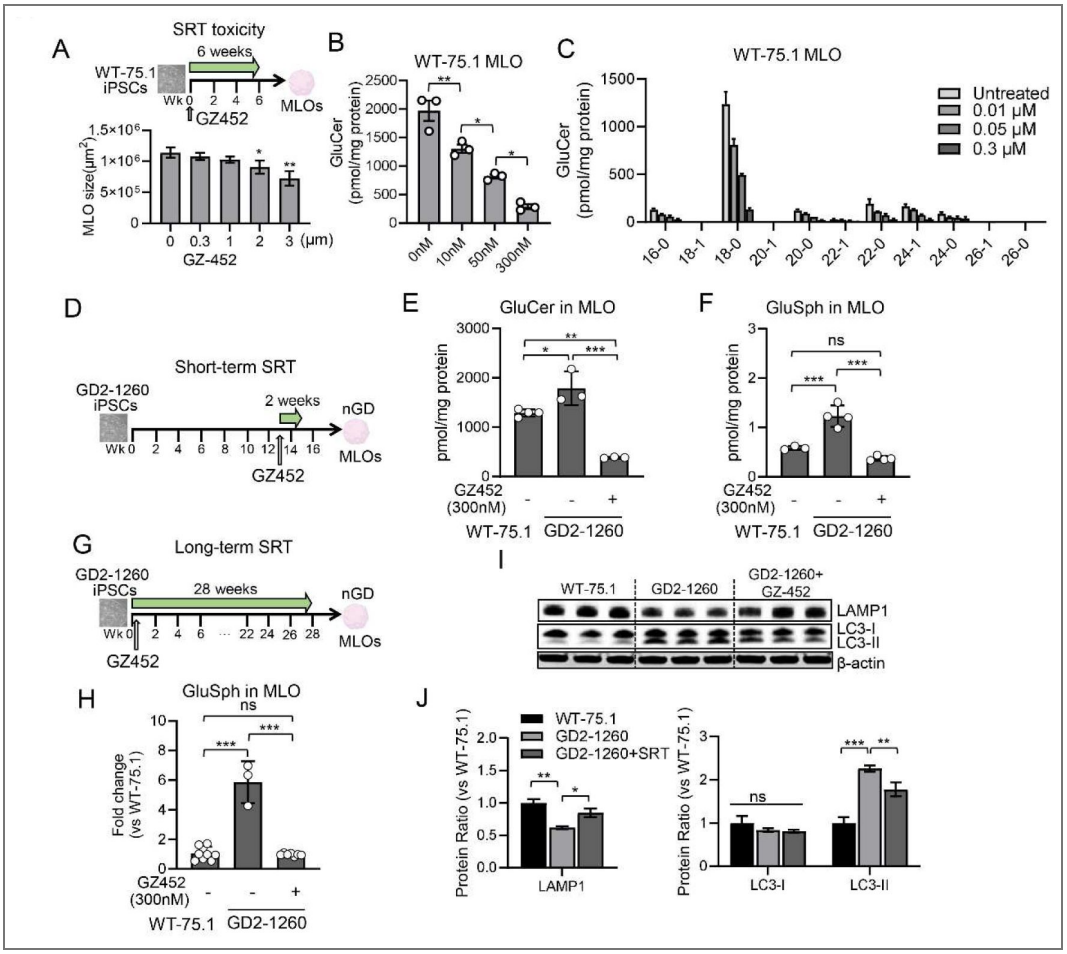

Figure 7. Substrate Reduction Therapy with GZ452 reduces lipid accumulation and improves autophagic and lysosomal abnormalities in GD MLOs.

(A) Assessment of GZ452 tolerated dose in healthy MLO and the effect of GZ452 on organoid growth in WT-75.1 MLOs over 6 weeks. Three MLOs were pooled and n = 3 per concentration. (B, C) Total GluCer levels (B) and distribution of GluCer species (C) in WT-75.1 MLOs with various doses of GZ452 at Wk6. Three MLOs were pooled and n = 3 per concentration. (D) Schematic of the experimental timeline for short-term (2 weeks) GZ452 treatment of GD MLOs. (E, F) GluCer (E) and GluSph (F) levels in WT-75.1 and GD2-1260 MLOs at Wk15 under short-term GZ452 treatment. Data were normalized to protein mass. (G) Schematic of the experimental timeline for long-term (28 weeks) GZ452 treatment in GD MLOs. (H) GluSph levels in MLOs at Wk15 under long-term GZ452 treatment. Data were normalized to protein mass. (I) Immunoblot analysis of LAMP1 and LC3-I/II in SRT treated GD2-1260 MLOs for 28 weeks, with β-actin as loading control. Protein samples were extracted from n=3 MLOs for each group. (J) Quantification of LAMP1 and LC3-II/I in MLOs. Protein levels are normalized to WT-75.1 untreated controls (set to 1.0). All data presented as mean ± SEM (n = 3~4). *p < 0.05; **p < 0.01; ns, not significant. One-way ANOVA with Tukey's test.

and normalized it to the WT level (Figure 7G, 7H). Immunoblot analysis showed that long-term GZ452 treatment improved lysosomal function, partially restoring LAMP1 levels (0.8 ± 0.1; $p < 0.05$) and reducing LC3-II by 21.4% ($p < 0.01$) (Figure 7I, 7J). These findings demonstrate that GZ452 effectively reduced lipid accumulation and improves lysosomal function in GD MLOs, supporting its therapeutic potential for ameliorating key disease phenotypes.

Discussion

We developed MLOs from two GD Type 2 patient-derived hiPSCs, offering deepened understanding to disease pathogenesis and an advanced model system for drug discovery. To our knowledge, this is the first GD brain organoid model derived from patient cells. These GD MLOs harbor prevalent *GBA1*$^{L444P/P415R}$ and *GBA1*$^{L444P/RecNcil}$ mutations, replicated key nGD phenotypes, including reduced GCase activity, glycosphingolipids accumulation, lysosomal abnormalities, and impaired dopaminergic neuron differentiation (Supplementary Table 2). Emerging interventions, CRISPR/Cas9-mediated gene correction, SapC-DOPS-fGCase nanoparticle, and AAV9-GBA1 gene therapy, significantly restored GCase function and mitigate disease hallmarks in GD MLOs, supporting their use in preclinical studies (Supplementary Table 2). Additionally, dysregulated Wnt signaling and impaired dopaminergic neuron differentiation in GD MLOs provides novel insights into nGD pathogenesis and potential therapeutic targets. This research underscores the utility of patient-derived MLOs as a human-relevant platform for modeling disease complexity and testing drug responses to bridge preclinical and clinical research.

Our findings revealed nGD-specific phenotypes in MLOs, including reduced GCase activity, GluCer and GluSph accumulation, and altered mTOR and autophagosome-lysosomal pathways, closely reflecting patient neuropathology [4,55]. Unlike *Gba1* knockout animal models, which lack patient-specific genetic and epigenetic diversity, patient-derived MLOs retain heterozygous or compound heterozygous background, enabling study of disease mechanisms and modifier genes. Partial rescue in isogenic iso-GD2-1260 MLOs, where mutation correction alleviated but did not fully resolve abnormalities, highlights the model's value in capturing nGD pathology and guiding personalized precision therapeutic strategies. This model offers a more advanced and physiologically relevant platform than traditional gene knockout or transgenic models, better capturing the complexity of nGD pathology.

Transcriptomic analysis of GD MLOs uncovered dysregulated Wnt signaling, a critical pathway in early brain development, highlighting a mechanistic insight into nGD pathogenesis. Aligning with Awad et al., who reported that downregulated Wnt/β-catenin signaling impairs DA neuron differentiation in nGD hiPSC-derived neuronal progenitors [30], our MLOs exhibited reduced FOXA2+ DA progenitors and TH+ mature DA neurons, along with decreased dopamine release in culture medium. Transcriptome analysis of the GD MLOs identified 1,429 differentially expressed genes enriched in Wnt signaling, axon guidance and neuron differentiation pathways, indicating that GCase deficiency disrupts midbrain patterning and neuronal specification. This finding is further supported by reduced expression of midbrain markers (e.g., FOXA2, TH), reduced dopamine release from DA neurons, and skewed forebrain/midbrain patterning genes (e.g., FOXP1, FOXG1) in GD MLOs. Compared to *GBA1* KO iPSC-derived midbrain-like organoids, which showed only a marginal reduction in dopaminergic neuron differentiation and no significant dysregulation of FOXG1 expression [24], our MLO model exhibits a distinct and more disease-relevant phenotype. These results suggest that aberrant Wnt signaling contributes to impaired dopaminergic neuron development and may drive the disease pathogenesis in nGD. Thus, targeting Wnt-related pathways could offer a therapeutic strategy to address early developmental defects in nGD. Comparative analysis with prior transcriptomic data from nGD mouse midbrain showed consistent dysregulation in axon guidance, synaptic signaling, lipid metabolism, and nervous system development etc. (Supplementary Table 3) [13], supporting the fidelity of our human MLO model. Moreover, midbrain organoids at 35 days of development closely correspond to the human embryonic midbrain at approximately 9 weeks, while 70-day-old organoids align more closely with the 10-week stage [64]. These correlations highlight the importance of initiating treatment during the fetal stage, which may be critical for preventing the disease.

Isogenic MLOs generated by correcting the *GBA1* L444P mutation in GD2-1260 hiPSCs using CRISPR/Cas9 revealed the key genetic mechanisms in nGD. The resulting WT/P415R genotype in iso-GD2-1260 partially rescued nGD phenotypes. GCase activity restored to nearly 50% of WT-75.1 levels, with normalized GluSph levels and improved TH expression. However, partial recovery of FOXA2 (53% of WT-75.1), along with persistent LC3 and LAMP1 abnormalities, may contribute to remaining pathology. These findings imply that the retained P415R mutation in this isogenic line may contribute to residual lysosomal dysfunction, potentially exerting a negative effect, as it has been reported to be associated with altered GCase stability and activity in previous studies [65,66]. The partial rescue in iso-GD2-1260 MLOs suggests that the P415R mutation may affect disease severity and therapeutic response, deserving further investigation into the specific role of P415R mutation in GD and assessing whether dual mutation correction is required for full phenotypic normalization.

Evaluation of GZ452, a CNS-accessible SRT drug [67], in GD2-1260 MLOs showed significant reduction in GluCer and GluSph levels at a well-tolerated dose, alongside partial restoration of lysosomal and autophagy markers (LAMP1, LC3-II). Unlike higher doses that affected organoid growth, 0.3 μM preserved MLO size and expression of midbrain markers (ASCL1, TH, PLZF) involved in organoid differentiation and growth. These findings underscore the value of the MLOs for assessing drug safety (e.g., organoid size as toxicity indicator) and efficacy in a human-specific, midbrain-relevant model before clinical studies. Our study demonstrated positive therapeutic outcomes using AAV9-GBA1 gene therapy and SapC-DOPS nanoparticle-mediated GCase delivery in GD2-1260 and GD2-10-257 MLOs. AAV9-GBA1 restored GCase activity, while SapC-DOPS-fGCase elevated GCase activity to WT levels, both approaches effectively reduced GluSph. Based on prior studies showing no region-specific effects in GD patients and mice, these therapies may also be effective in other brain organoid types, such as COs [4,41]. The novelty of employing MLOs lies in their ability to concurrently test these diverse therapeutic modalities: SRT, gene therapy, and nanoparticle-based enzyme delivery within a patient-derived system that replicates nGD pathology, offering the unique patient-MLO system to assess complex cellular responses that directly reflect patient specific conditions.

Unlike animal models, MLOs provide a controlled environment to evaluate dose-dependent effects and cellular responses, enabling the identification of optimal therapeutic windows while minimizing the risk of adverse outcomes in patients with nGD. Moreover, FDA has increasingly encouraged the use of organoid systems in drug development, recognizing their potential to improve preclinical testing and reduce reliance on animal models. Therefore, the adaptability of MLOs to test advanced interventions, coupled with their alignment with regulatory trends favoring human-relevant models, positions them as a great tool for accelerating the translation of innovative treatments from preclinical research to clinical application.

There are limitations in our current MLOs, such as lacking vascular system and microglia. The absence of microglia and vasculature may contribute to incomplete phenotyping and phenotypic rescue observed in our therapeutic experiments. Without vascularization, cells in the core may experience hypoxic and nutrient deprivation, leading cell death or necrosis in deeper layers in long-term culture. This limitation may partially explain the incomplete restoration of dopaminergic markers (TH, FOXA2) and partial recovery of LAMP1 following SapC-DOPS-fGCase and AAV9-GBA1 treatments. Additionally, the lack of microglia limits molding of neuroinflammatory, which contributes to the clearance of toxic lipid substrates and mediating neuronal damage in GD. Elevated GluSph and impaired dopaminergic differentiation observed in GD MLOs may not fully reflect inflammatory process. Dysregulated Wnt signaling and lysosomal and autophagic markers (LAMP1, LC3-II/I) could be amplified by microglial activation *in vivo*. To improve model fidelity, future studies would incorporate vascularization (e.g., endothelial co-culture or microfluidics) to enhance oxygen and nutrient distribution and integrate microglia via directed differentiation [68] or co-culture with hiPSC-derived microglia [69] to enhance the relevance of MLOs for long-term nGD research and drug testing.

In conclusion, patient-derived MLOs offer an advanced, human-relevant platform for elucidating nGD pathogenesis and evaluating therapies, overcoming limitations of traditional models. Dysregulated Wnt signaling and impaired dopaminergic neuron differentiation, along with partial rescue of phenotypes through gene correction, highlight the complex genetic and developmental underpinnings of nGD. The efficacy assessment of SapC-DOPS-fGCase, AAV9-GBA1 and SRT-GZ452 therapies underscores the targeted interventions and safety evaluation of these approaches in patient-derived brain organoid models. While limitations such as lack of vascularization and microglia constrain modeling of neuroinflammation, these challenges can be addressed as discussed above and using advanced culturing techniques. Collectively, our findings lay the groundwork for developing patient-specific preclinical models to support personalized therapeutic strategies, while also advocating for the continued refinement of MLO systems to accelerate the discovery of effective treatments for nGD.

Data availability

RNA sequence data were deposited in GEO (accession number GSE303993). All data generated or analyzed during this study are included in the manuscript and supporting files; source data files have been provided for all figures.

Acknowledgements

This work was supported by the Cincinnati Children's Pluripotent Stem Cell Facility (*RRID:SCR_022634*), Clinical and Biomedical Mass Spectrometry Facility (*RRID:SCR_022638*) and Transgenic Animal and Genome Editing Facility (*RRID:SCR_022642*). Authors acknowledge Freeline Therapeutics (now Spur Therapeutics) for providing the fGCase under a Material Transfer Agreement.

Additional information

Funding

This work is supported by awards from the National Institute of Health (grant number R21HD1027881, R21OD033660 and R01NS138309 to Y.S.; R01NS103931 partly to Y.S.; R21HD1027881 partly to C.N.M.; R01NS138309 partly to X.Q.); the National Center for Advancing Translational Sciences of the National Institutes of Health (Award Number 2UL1TR001425-05A1, CHMC-CTSA 00003827 to Y.S.); Cincinnati Children's Hospital Medical Center (CCHMC) Center of Pediatric Genomics Award to Y.S.; CCHMC Research Innovation Pilot Funding Program Award to Y.S., Y.L. and J.E.H. The funding source did not have any role in study design, data collection, data analyses, interpretation, or writing of report.

Author Contributions

Y.L. designed experiments, cultured hiPSCs and MLOs, performed experiments, analyzed data, and wrote the manuscript. B.L. measured GCase enzyme activity in hiPSCs and MLOs. V.F. carried out lipid extract from hiPSCs and MLOs, W.Z., X.Z., R.L.B. and K.DR.S performed quantification of GluCer/GluSph by LC-MS/MS and data analysis. S.A. assisted with immunofluorescence staining and immunoblot assays. C.N.M and YC.H made isogenic hiPSC cells and conceived experimental designs and edited the manuscript. J.T. conceived experimental designs and edited the manuscript. J.E.H. generated cerebral organoid and edited manuscript. A.K. and X.Q. provided SapC-DOPS nanoparticles and guidance for the enzyme uptake assay. R.A.F provided an nGD hiPSC cell line and edited the manuscript. Y.S. conceived experimental designs, supervised the project, wrote the manuscript, and provided funding to the study.

Ethics

This work has been reviewed and approved by the Cincinnati Children's Hospital Medical Center (CCHMC) and University of Cincinnati (UC) Embryonic Stem Cell Research Oversight (ESCRO) committee under ESCRO protocol #EIPHG3114_R3. Primary fibroblast (GM01260) for generating GD2-1260 iPSC was obtained from the Coriell Institute for Medical Research under Material Transfer Agreement. WT-75.1 iPSC was generated using fibroblasts cultured from discarded circumcision tissue obtained from a healthy donor (provided by Dr. Susanne Wells, Division of Hematology/Oncology, CCHMC; institutional review board no. 02-9-29X) at CCHMC. The procedures used to generate the GD2-1260 iPSC and WT-75.1 iPSC lines at CCHMC have been reviewed and approved by CCHMC/UC ESCRO committee. Skin biopsies to generate GD2-10-257 iPSCs were obtained from NIH with informed consent and were approved by the Institutional Review Board (IRB). The procedures used to generate the GD-2-10-257 nGD iPSC line at the University of Maryland Baltimore (UMB) have been reviewed and approved by the UMB IRB and ESCRO committees.

Funding

Funder	Grant reference number	Author
National Institutes of Health	R21HD1027881	Christopher N Mayhew Ying Sun
National Institutes of Health	R21OD033660	Ying Sun
National Institutes of Health	R01NS138309	Xiaoyang Qi Ying Sun
National Institutes of Health	R01NS103931	Ying Sun
National Institutes of Health	2UL1TR001425-05A1	Ying Sun
Cincinnati Children's Hospital Medical Center (CCHMC)	Center of Pediatric Genomics Award	Ying Sun
Cincinnati Children's Hospital Medical Center (CCHMC)	Research Innovation Pilot Funding Program Award	Jason E Hammonds Ying Sun Yi Lin

Author ORCID iDs

Ricardo A Feldman: https://orcid.org/0000-0001-6090-0439
Ying Sun: https://orcid.org/0000-0002-2979-4735

Additional files

supplemental file

References

1. **Grabowski G.A.,** Petsko G.A., Kolodny E.H (2010) Gaucher disease. In: Valle D., Beaudet A., Vogelstein B., Kinzler K.W., Antonarakis S.E., Ballabio A., Scriver C.R., Sly W.S., Childs B., Bunz F. (Eds). *The Online Metabolic and Molecular Bases of Inherited Diseases* New York: The McGraw-Hill Companies, Inc.
2. **Mignot C.,** Gelot A., Bessieres B., Daffos F., Voyer M., Menez F., Fallet Bianco C., Odent S., Le Duff D., Loget P., *et al.* (2003) Perinatal-lethal Gaucher disease. *American journal of medical genetics Part A* **120A**:338-344 https://doi.org/10.1002/ajmg.a.20117 | PubMed
3. **Reissner K.,** Tayebi N., Stubblefield B.K., Koprivica V., Blitzer M., Holleran W., Cowan T., Almashanu S., Maddalena A., Karson E.M., *et al.* (1998) Type 2 Gaucher disease with hydrops fetalis in an Ashkenazi Jewish family resulting from a novel recombinant allele and a rare splice junction mutation in the

glucocerebrosidase locus. *Molecular genetics and metabolism* **63**:281-288 https://doi.org/10.1006/mgme.1998.2675 | PubMed

4. **Burrow T.A.,** Sun Y., Prada C.E., Bailey L., Zhang W., Brewer A., Wu S.W., Setchell K.D.R., Witte D., Cohen M.B., *et al.* (2015) CNS, lung, and lymph node involvement in Gaucher disease type 3 after 11 years of therapy: clinical, histopathologic, and biochemical findings. *Molecular genetics and metabolism* **114**:233-241 https://doi.org/10.1016/j.ymgme.2014.08.011 | PubMed

5. **Wong K.,** Sidransky E., Verma A., Mixon T., Sandberg G.D., Wakefield L.K., Morrison A., Lwin A., Colegial C., Allman J.M., *et al.* (2004) Neuropathology provides clues to the pathophysiology of Gaucher disease. *Molecular genetics and metabolism* **82**:192-207 https://doi.org/10.1016/j.ymgme.2004.04.011 | PubMed

6. **Conradi N.G.,** Sourander P., Nilsson O., Svennerholm L., Erikson A (1984) Neuropathology of the Norrbottnian type of Gaucher disease. Morphological and biochemical studies. *Acta neuropathologica* **65**:99-109 https://doi.org/10.1007/bf00690463 | PubMed

7. **Enquist I.B.,** Lo Bianco C., Ooka A., Nilsson E., Mansson J.E., Ehinger M., Richter J., Brady R.O., Kirik D., Karlsson S (2007) Murine models of acute neuronopathic Gaucher disease. *Proceedings of the National Academy of Sciences of the United States of America* **104**:17483-17488 https://doi.org/10.1073/pnas.0708086104 | PubMed

8. **Vardi A.,** Zigdon H., Meshcheriakova A., Klein A.D., Yaacobi C., Eilam R., Kenwood B.M., Rahim A.A., Massaro G., Merrill A.H., *et al.* (2016) Delineating pathological pathways in a chemically induced mouse model of Gaucher disease. *J Pathol* **239**:496-509 https://doi.org/10.1002/path.4751 | PubMed

9. **Xu Y.H.,** Reboulet R., Quinn B., Huelsken J., Witte D., Grabowski G.A (2008) Dependence of reversibility and progression of mouse neuronopathic Gaucher disease on acid beta-glucosidase residual activity levels. *Molecular genetics and metabolism* **94**:190-203 https://doi.org/10.1016/j.ymgme.2008.01.013 | PubMed

10. **Xu Y.H.,** Quinn B., Witte D., Grabowski G.A (2003) Viable mouse models of acid beta-glucosidase deficiency: the defect in Gaucher disease. *Am J Pathol* **163**:2093-2101 https://doi.org/10.1016/s0002-9440(10)63566-3

11. **Sun Y.,** Liou B., Ran H., Skelton M.R., Williams M.T., Vorhees C.V., Kitatani K., Hannun Y.A., Witte D.P., Xu Y.H., *et al.* (2010) Neuronopathic Gaucher disease in the mouse: viable combined selective saposin C deficiency and mutant glucocerebrosidase (V394L) mice with glucosylsphingosine and glucosylceramide accumulation and progressive neurological deficits. *Human molecular genetics* **19**:1088-1097 https://doi.org/10.1093/hmg/ddp580 | PubMed

12. **Qi X.,** Leonova T., Grabowski G.A (1994) Functional human saposins expressed in Escherichia coli. Evidence for binding and activation properties of saposins C with acid beta-glucosidase. *J Biol Chem* **269**:16746-16753 https://doi.org/10.1016/s0021-9258(19)89454-1 | PubMed

13. **Dasgupta N.,** Xu Y.H., Li R., Peng Y., Pandey M.K., Tinch S.L., Liou B., Inskeep V., Zhang W., Setchell K.D., *et al.* (2015) Neuronopathic Gaucher disease: dysregulated mRNAs and miRNAs in brain pathogenesis and effects of pharmacologic chaperone treatment in a mouse model. *Human molecular genetics* **24**:7031-7048 https://doi.org/10.1093/hmg/ddv404 | PubMed

14. **Liu Y.,** Suzuki K., Reed J.D., Grinberg A., Westphal H., Hoffmann A., Doring T., Sandhoff K., Proia R.L (1998) Mice with type 2 and 3 Gaucher disease point mutations generated by a single insertion mutagenesis procedure. *Proceedings of the National Academy of Sciences of the United States of America* **95**:2503-2508 https://doi.org/10.1073/pnas.95.5.2503 | PubMed

15. **Pasmanik-Chor M.,** Laadan S., Elroy-Stein O., Zimran A., Abrahamov A., Gatt S., Horowitz M (1996) The glucocerebrosidase D409H mutation in Gaucher disease. *Biochemical and molecular medicine* **59**:125-133 https://doi.org/10.1006/bmme.1996.0077 | PubMed

16. **Grabowski G.A.,** Zimran A., Ida H (2015) Gaucher disease types 1 and 3: Phenotypic characterization of large populations from the ICGG Gaucher Registry. *American journal of hematology* **90**:S12-18 https://doi.org/10.1002/ajh.24063 | PubMed

17. **Birtele M.,** Lancaster M., Quadrato G (2025) Modelling human brain development and disease with organoids. *Nat Rev Mol Cell Biol* **26**:389-412 https://doi.org/10.1038/s41580-024-00804-1 | PubMed

18. **Di Lullo E.,** Kriegstein A.R. (2017) The use of brain organoids to investigate neural development and disease. *Nature reviews. Neuroscience* **18**:573-584 https://doi.org/10.1038/nrn.2017.107 | PubMed

19. **Raja W.K.,** Mungenast A.E., Lin Y.T., Ko T., Abdurrob F., Seo J., Tsai L.H (2016) Self-Organizing 3D Human Neural Tissue Derived from Induced Pluripotent Stem Cells Recapitulate Alzheimer's Disease Phenotypes. *PLoS One* **11**:e0161969 https://doi.org/10.1371/journal.pone.0161969 | PubMed

20. **Lancaster M.A.,** Renner M., Martin C.A., Wenzel D., Bicknell L.S., Hurles M.E., Homfray T., Penninger J.M., Jackson A.P., Knoblich J.A (2013) Cerebral organoids model human brain development and microcephaly. *Nature* **501**:373-379 https://doi.org/10.1038/nature12517 | PubMed

21. **Smits L.M.,** Reinhardt L., Reinhardt P., Glatza M., Monzel A.S., Stanslowsky N., Rosato-Siri M.D., Zanon A., Antony P.M., Bellmann J., *et al.* (2019) Modeling Parkinson's disease in midbrain-like organoids. *NPJ Parkinson's disease* **5**:5 https://doi.org/10.1038/s41531-019-0078-4 | PubMed

22. **Allende M.L.,** Cook E.K., Larman B.C., Nugent A., Brady J.M., Golebiowski D., Sena-Esteves M., Tifft C.J., Proia R.L (2018) Cerebral organoids derived from Sandhoff disease-induced pluripotent stem cells exhibit impaired neurodifferentiation. *J Lipid Res* **59**:550-563 https://doi.org/10.1194/jlr.M081323 | PubMed

23. **Latour Y.L.,** Yoon R., Thomas S.E., Grant C., Li C., Sena-Esteves M., Allende M.L., Proia R.L., Tifft C.J (2019) Human GLB1 knockout cerebral organoids: A model system for testing AAV9-mediated GLB1 gene therapy for reducing GM1 ganglioside storage in GM1 gangliosidosis. *Mol Genet Metab Rep* **21**:100513 https://doi.org/10.1016/j.ymgmr.2019.100513 | PubMed

24. **Jo J.,** Yang L., Tran H.D., Yu W., Sun A.X., Chang Y.Y., Jung B.C., Lee S.J., Saw T.Y., Xiao B., *et al.* (2021) Lewy Body-like Inclusions in Human Midbrain Organoids Carrying Glucocerebrosidase and alpha-Synuclein Mutations. *Ann Neurol* **90**:490-505 https://doi.org/10.1002/ana.26166 | PubMed

25. **Goker-Alpan O.,** Ivanova M.M (2024) Neuronopathic Gaucher disease: Rare in the West, common in the East. *J Inherit Metab Dis* **47**:917-934 https://doi.org/10.1002/jimd.12749 | PubMed

26. **Farfel-Becker T.,** Vitner E.B., Kelly S.L., Bame J.R., Duan J., Shinder V., Merrill A.H., Dobrenis K., Futerman A.H (2014) Neuronal accumulation of glucosylceramide in a mouse model of neuronopathic Gaucher disease leads to neurodegeneration. *Human molecular genetics* **23**:843-854 https://doi.org/10.1093/hmg/ddt468 | PubMed

27. **Jones E.E.,** Zhang W., Zhao X., Quiason C., Dale S., Shahidi-Latham S., Grabowski G.A., Setchell K.D.R., Drake R.R., Sun Y (2017) Tissue Localization of Glycosphingolipid Accumulation in a Gaucher Disease Mouse Brain by LC-ESI-MS/MS and High-Resolution MALDI Imaging Mass Spectrometry. *SLAS Discov* **22**:1218-1228 https://doi.org/10.1177/2472555217719372 | PubMed

28. **Xu Y.H.,** Xu K., Sun Y., Liou B., Quinn B., Li R.H., Xue L., Zhang W., Setchell K.D., Witte D., *et al.* (2014) Multiple pathogenic proteins implicated in neuronopathic Gaucher disease mice. *Human molecular genetics* **23**:3943-3957 https://doi.org/10.1093/hmg/ddu105 | PubMed

29. **Sun Y.,** Florer J., Mayhew C.N., Jia Z., Zhao Z., Xu K., Ran H., Liou B., Zhang W., Setchell K.D., *et al.* (2015) Properties of neurons derived from induced pluripotent stem cells of Gaucher disease type 2 patient fibroblasts: potential role in neuropathology. *PLoS One* **10**:e0118771 https://doi.org/10.1371/journal.pone.0118771 | PubMed

30. **Awad O.,** Panicker L.M., Deranieh R.M., Srikanth M.P., Brown R.A., Voit A., Peesay T., Park T.S., Zambidis E.T., Feldman R.A (2017) Altered Differentiation Potential of Gaucher's Disease iPSC Neuronal Progenitors due to Wnt/beta-Catenin Downregulation. *Stem Cell Reports* **9**:1853-1867 https://doi.org/10.1016/j.stemcr.2017.10.029 | PubMed

31. **Kwak T.H.,** Kang J.H., Hali S., Kim J., Kim K.P., Park C., Lee J.H., Ryu H.K., Na J.E., Jo J., *et al.* (2020) Generation of homogeneous midbrain organoids with in vivo-like cellular composition facilitates neurotoxin-based Parkinson's disease modeling. *Stem cells* **38**:727-740 https://doi.org/10.1002/stem.3163 | PubMed

32. **Jo J.,** Xiao Y., Sun A.X., Cukuroglu E., Tran H.D., Goke J., Tan Z.Y., Saw T.Y., Tan C.P., Lokman H., *et al.* (2016) Midbrain-like Organoids from Human Pluripotent Stem Cells Contain Functional Dopaminergic and Neuromelanin-Producing Neurons. *Cell stem cell* **19**:248-257 https://doi.org/10.1016/j.stem.2016.07.005 | PubMed

33. **Ran F.A.,** Hsu P.D., Wright J., Agarwala V., Scott D.A., Zhang F (2013) Genome engineering using the CRISPR-Cas9 system. *Nat Protoc* **8**:2281-2308 https://doi.org/10.1038/nprot.2013.143 | PubMed

34. **Chen B.,** Gilbert L.A., Cimini B.A., Schnitzbauer J., Zhang W., Li G.W., Park J., Blackburn E.H., Weissman J.S., Qi L.S., *et al.* (2013) Dynamic imaging of genomic loci in living human cells by an optimized CRISPR/Cas system. *Cell* **155**:1479-1491 https://doi.org/10.1016/j.cell.2013.12.001 | PubMed

35. **Horowitz M.,** Wilder S., Horowitz Z., Reiner O., Gelbart T., Beutler E (1989) The human glucocerebrosidase gene and pseudogene: structure and evolution. *Genomics* **4**:87-96 https://doi.org/10.1016/0888-7543(89)90319-4 | PubMed

36. **Woo E.G.,** Tayebi N., Sidransky E (2021) Next-Generation Sequencing Analysis of GBA1: The Challenge of Detecting Complex Recombinant Alleles. *Front Genet* **12**:684067 https://doi.org/10.3389/fgene.2021.684067 | PubMed

37. **Hsu P.D.,** Scott D.A., Weinstein J.A., Ran F.A., Konermann S., Agarwala V., Li Y., Fine E.J., Wu X., Shalem O., *et al.* (2013) DNA targeting specificity of RNA-guided Cas9 nucleases. *Nature Biotechnology* **31**:827-832 https://doi.org/10.1038/nbt.2647 | PubMed

38. **Sun Y.,** Liou B., Chu Z., Fannin V., Blackwood R., Peng Y., Grabowski G.A., Davis H.W., Qi X (2020) Systemic enzyme delivery by blood-brain barrier-penetrating SapC-DOPS nanovesicles for treatment of neuronopathic Gaucher disease. *EBioMedicine* **55**:102735 https://doi.org/10.1016/j.ebiom.2020.102735 | PubMed

39. **Zhao S.,** Chu Z., Blanco V.M., Nie Y., Hou Y., Qi X. (2015) SapC-DOPS nanovesicles as targeted therapy for lung cancer. *Mol Cancer Ther* **14**:491-498 https://doi.org/10.1158/1535-7163.MCT-14-0661 | PubMed

40. **Marshall J.,** Sun Y., Bangari D.S., Budman E., Park H., Nietupski J.B., Allaire A., Cromwell M.A., Wang B., Grabowski G.A., *et al.* (2016) CNS-accessible Inhibitor of Glucosylceramide Synthase for Substrate Reduction Therapy of Neuronopathic Gaucher Disease. *Mol Ther* **24**:1019-1029 https://doi.org/10.1038/mt.2016.53 | PubMed

41. **Sun Y.,** Zhang W., Xu Y.H., Quinn B., Dasgupta N., Liou B., Setchell K.D., Grabowski G.A (2013) Substrate compositional variation with tissue/region and Gba1 mutations in mouse models--implications for Gaucher disease. *PLoS One* **8**:e57560 https://doi.org/10.1371/journal.pone.0057560 | PubMed

42. **Zhang W.,** Oehrle M., Prada C.E., Schwartz I.V.D., Chutipongtanate S., Wattanasirichaigoon D., Inskeep V., Dai M., Pan D., Sun Y., *et al.* (2017) A convenient approach to facilitate monitoring Gaucher disease progression and therapeutic response. *The Analyst* **142**:3380-3387 https://doi.org/10.1039/c7an00938k | PubMed

43. **Zhao X.,** Lin Y., Liou B., Fu W., Jian J., Fannie V., Zhang W., Setchell K.D.R., Grabowski G.A., Sun Y., *et al.* (2023) PGRN deficiency exacerbates, whereas a brain penetrant PGRN derivative protects, GBA1 mutation-associated pathologies and diseases. *Proceedings of the National Academy of Sciences of the United States of America* **120**:e2210442120 https://doi.org/10.1073/pnas.2210442120 | PubMed

44. **Love M.I.,** Huber W., Anders S (2014) Moderated estimation of fold change and dispersion for RNA-seq data with DESeq2. *Genome Biol* **15**:550 https://doi.org/10.1186/s13059-014-0550-8 | PubMed

45. **Sherman B.T.,** Hao M., Qiu J., Jiao X., Baseler M.W., Lane H.C., Imamichi T., Chang W (2022) DAVID: a web server for functional enrichment analysis and functional annotation of gene lists (2021 update). *Nucleic Acids Res* **50**:W216-W221 https://doi.org/10.1093/nar/gkac194 | PubMed

46. **Dai M.,** Lin Y., El-Amouri S.S., Kohls M., Pan D (2018) Comprehensive evaluation of blood-brain barrier-forming micro-vasculatures: Reference and marker genes with cellular composition. *PLoS One* **13**:e0197379 https://doi.org/10.1371/journal.pone.0197379 | PubMed

47. **Prakash N.,** Wurst W (2006) Genetic networks controlling the development of midbrain dopaminergic neurons. *J Physiol* **575**:403-410 https://doi.org/10.1113/jphysiol.2006.113464 | PubMed

48. **Green D.,** Whitener A.E., Mohanty S., Lekven A.C (2015) Vertebrate nervous system posteriorization: Grading the function of Wnt signaling. *Dev Dyn* **244**:507-512 https://doi.org/10.1002/dvdy.24230 | PubMed

49. **Ryckman A.E.,** Brockhausen I., Walia J.S (2020) Metabolism of Glycosphingolipids and Their Role in the Pathophysiology of Lysosomal Storage Disorders. *Int J Mol Sci* **21** https://doi.org/10.3390/ijms21186881 | PubMed

50. **Srikanth M.P.,** Jones J.W., Kane M., Awad O., Park T.S., Zambidis E.T., Feldman R.A (2021) Elevated glucosylsphingosine in Gaucher disease induced pluripotent stem cell neurons deregulates lysosomal compartment through mammalian target of rapamycin complex 1. *Stem Cells Transl Med* **10**:1081-1094 https://doi.org/10.1002/sctm.20-0386 | PubMed

51. **Mato-Blanco X.,** Kim S.K., Jourdon A., Ma S., Choi S.H., Giani A.M., Paredes M.I., Tebbenkamp A.T.N., Liu F., Duque A., *et al.* (2025) Early developmental origins of cortical disorders modeled in human neural stem cells. *Nat Commun* **16** https://doi.org/10.1038/s41467-025-61316-w | PubMed

52. **Ba R.,** Yang L., Zhang B., Jiang P., Ding Z., Zhou X., Yang Z., Zhao C (2023) FOXG1 drives transcriptomic networks to specify principal neuron subtypes during the development of the medial pallium. *Sci Adv* **9**:eade2441 https://doi.org/10.1126/sciadv.ade2441 | PubMed

53. **Ortiz A.,** Ayhan F., Khandelwal N., Outland E., Jankovic M., Harper M., Konopka G (2025) Cell-type-specific roles of FOXP1 in the excitatory neuronal lineage during early neocortical murine development. *Cell Rep* **44**:115384 https://doi.org/10.1016/j.celrep.2025.115384 | PubMed

54. **Peng Y.,** Liou B., Lin Y., Mayhew C.N., Fleming S.M., Sun Y (2023) iPSC-derived neural precursor cells engineering GBA1 recovers acid beta-glucosidase deficiency and diminishes alpha-synuclein and neuropathology. *Mol Ther Methods Clin Dev* **29**:185-201 https://doi.org/10.1016/j.omtm.2023.03.007 | PubMed

55. **Brown R.A.,** Voit A., Srikanth M.P., Thayer J.A., Kingsbury T.J., Jacobson M.A., Lipinski M.M., Feldman R.A., Awad O (2019) mTOR hyperactivity mediates lysosomal dysfunction in Gaucher's disease iPSC-neuronal cells. *Dis Model Mech* **12** https://doi.org/10.1242/dmm.038596 | PubMed

56. **Panicker L.M.,** Miller D., Park T.S., Patel B., Azevedo J.L., Awad O., Masood M.A., Veenstra T.D., Goldin E., Stubblefield B.K., *et al.* (2012) Induced pluripotent stem cell model recapitulates pathologic hallmarks of Gaucher disease. *Proceedings of the National Academy of Sciences of the United States of America* **109**:18054-18059 https://doi.org/10.1073/pnas.1207889109 | PubMed

57. **Comper F.,** Miranda C.J., Liou B., Dodev T., Jeyakumar J.M., Canavese M., Cocita C., Khoshrou K., Tiscornia G., Chisari E., *et al.* (2025) FLT201, a novel liver-directed AAV gene therapy candidate for Gaucher disease type 1. *Mol Ther* **33**:3789-3807 https://doi.org/10.1016/j.ymthe.2025.05.003 | PubMed

58. **Hughes D.A.,** Ferrante F (2023) GALILEO-1: A Phase I/II safety and efficacy study of FLT201 gene therapy for Gaucher disease type 1. *Future Rare Diseases* **3** https://doi.org/10.2217/frd-2022-0019

59. **Al-Zaidy S.,** Pickard A.S., Kotha K., Alfano L.N., Lowes L., Paul G., Church K., Lehman K., Sproule D.M., Dabbous O., *et al.* (2019) Health outcomes in spinal muscular atrophy type 1 following AVXS-101 gene replacement therapy. *Pediatr Pulmonol* **54**:179-185 https://doi.org/10.1002/ppul.24203 | PubMed

60. **Drag S.,** Dotiwala F., Upadhyay A.K (2023) Gene Therapy for Retinal Degenerative Diseases: Progress, Challenges, and Future Directions. *Invest Ophthalmol Vis Sci* **64** https://doi.org/10.1167/iovs.64.7.39 | PubMed

61. **Aerts J.M.,** Hollak C.E., Boot R.G., Groener J.E., Maas M (2006) Substrate reduction therapy of glycosphingolipid storage disorders. *J Inherit Metab Dis* **29**:449-456 https://doi.org/10.1007/s10545-006-0272-5 | PubMed

62. **Scott L.J** (2015) Eliglustat: A Review in Gaucher Disease Type 1. *Drugs* **75**:1669-1678 https://doi.org/10.1007/s40265-015-0468-9 | PubMed

63. **Schiffmann R.,** Mengel E., Wallace M., Rochmann C., Turnbull J., Krupnick R., Gwaltney C., Pulikottil-Jacob R., Batsu I., Zheng R., *et al.* (2024) Qualitative Study of the Patient Experience with Venglustat for Gaucher Disease Type 3 in a Phase 2 Open-Label, Multicenter, Multinational Study (LEAP). *Adv Ther* **41**:2907-2923 https://doi.org/10.1007/s12325-024-02881-2 | PubMed

64. **Zagare A.,** Barmpa K., Smajic S., Smits L.M., Grzyb K., Grunewald A., Skupin A., Nickels S.L., Schwamborn J.C (2022) Midbrain organoids mimic early embryonic neurodevelopment and recapitulate LRRK2-p.Gly2019Ser-associated gene expression. *Am J Hum Genet* **109**:311-327 https://doi.org/10.1016/j.ajhg.2021.12.009 | PubMed

65. **Grace M.E.,** Berg A., He G.S., Goldberg L., Horowitz M., Grabowski G.A (1991) Gaucher disease: heterologous expression of two alleles associated with neuronopathic phenotypes. *Am J Hum Genet* **49**:646-655 PubMed

66. **Ron I.,** Dagan A., Gatt S., Pasmanik-Chor M., Horowitz M (2005) Use of fluorescent substrates for characterization of Gaucher disease mutations. *Blood Cells Mol Dis* **35**:57-65 https://doi.org/10.1016/j.bcmd.2005.03.006 | PubMed

67. **Peng Y.,** Liou B., Lin Y., Fannin V., Zhang W., Feldman R.A., Setchell K.D.R., Grabowski G.A., Sun Y (2021) Substrate Reduction Therapy Reverses Mitochondrial, mTOR, and Autophagy Alterations in a Cell Model of Gaucher Disease. *Cells* **10** https://doi.org/10.3390/cells10092286 | PubMed

68. **Cakir B.,** Tanaka Y., Kiral F.R., Xiang Y., Dagliyan O., Wang J., Lee M., Greaney A.M., Yang W.S., duBoulay C., *et al.* (2022) Expression of the transcription factor PU.1 induces the generation of microglia-like cells in human cortical organoids. *Nat Commun* **13**:430 https://doi.org/10.1038/s41467-022-28043-y | PubMed

69. **Sabate-Soler S.,** Nickels S.L., Saraiva C., Berger E., Dubonyte U., Barmpa K., Lan Y.J., Kouno T., Jarazo J., Robertson G., *et al.* (2022) Microglia integration into human midbrain organoids leads to increased neuronal maturation and functionality. *Glia* **70**:1267-1288 https://doi.org/10.1002/glia.24167 | PubMed

Peer reviews

Reviewer #1 (Public review):

In this study, the authors set out to develop a human disease model using stem cell-derived systems and to use this platform to investigate disease biology and evaluate potential therapeutic approaches. Their goal is to provide a tractable experimental system that captures key features of the disease and enables testing of candidate interventions.

The work has several important strengths. The authors present a carefully constructed model with improved genetic replication and clearer reporting of biological replicates, which enhances confidence in the reproducibility of the findings. The longitudinal design, spanning early developmental stages to later disease-relevant phenotypes, provides a useful framework for distinguishing temporal aspects of the disease process. The study also includes a comparative evaluation of multiple therapeutic strategies adding practical value to the field. In addition, statistical reporting and transparency have been strengthened, and key limitations of the model-such as the absence of certain cell types-are now clearly acknowledged.

At the same time, notable weaknesses temper the strength of the conclusions. Several central biological claims, particularly those related to specific signaling pathways, are supported primarily by transcriptomic and protein-level observations without direct functional validation. Similarly, measures used to interpret cellular processes do not fully distinguish between alternative biological explanations, leaving some mechanistic interpretations unresolved. The therapeutic findings are supported by biochemical changes, but evidence for functional recovery at the cellular level is limited. These gaps mean that some of the broader conclusions should be interpreted with caution.

Overall, the authors have largely achieved their aim of establishing a useful experimental model and demonstrating its potential for studying disease-related changes and testing interventions. The evidence is convincing for the descriptive and comparative aspects of the work, but more limited for mechanistic and functional claims.

The study is likely to have a meaningful impact by providing a platform that others in the field can build upon. The methods and datasets will be useful to researchers interested in disease modeling and therapeutic development. At the same time, the work is best viewed as an important foundation, with key mechanistic and functional questions remaining to be addressed in future studies.

https://doi.org/10.7554/eLife.109518.2.sa3

Reviewer #2 (Public review):

Sun et al. have developed a midbrain-like organoid (MLO) model for neuronopathic Gaucher disease (nGD). The MLOs recapitulate several features of nGD molecular pathology, including reduced GCase activity, sphingolipid accumulation, and impaired dopaminergic neuron development. They also characterize the transcriptome in the MLO nGD model. CRISPR correction of one of the GBA1 mutant alleles rescues most of the nGD molecular phenotypes. The MLO model was further deployed in proof-of-principle studies of investigational nGD therapies, including SapC-DOPS nanovesicles, AAV9-mediated GBA1 gene delivery, and substrate-reduction therapy (GZ452). This patient-specific 3D model provides a new platform for studying nGD mechanisms and accelerating therapy development. Overall, only modest weaknesses are noted, and these have been adequately addressed in the revision.

Comments on revisions:

I have no further recommendations. The revised manuscript addresses the few questions and concerns that I had initially shared.

https://doi.org/10.7554/eLife.109518.2.sa2

Reviewer #3 (Public review):

Summary:

In this study, the authors describe modeling of neuronopathic Gaucher disease (nGD) using midbrain-like organoids (MLOs) derived from hiPSCs carrying GBA1 L444P/P415R or L444P/RecNciI variants. These MLOs recapitulate several disease features, including GCase deficiency, reduced enzymatic activity, lipid substrate accumulation, and impaired dopaminergic neuron differentiation. Correction of the GBA1 L444P variant restored GCase activity, normalized lipid metabolism, and rescued dopaminergic neuronal defects, confirming its pathogenic role in the MLO model. The authors further leveraged this system to evaluate therapeutic strategies, including: (i) SapC-DOPS nanovesicles for GCase delivery, (ii) AAV9-mediated GBA1 gene therapy, and (iii) GZ452, a glucosylceramide synthase inhibitor. These treatments reduced lipid accumulation and ameliorated autophagic, lysosomal, and neurodevelopmental abnormalities.

Strengths:

This manuscript demonstrates that nGD patient-derived MLOs can serve as an additional platform for investigating nGD mechanisms and advancing therapeutic development.

Comments on revisions:

I have no further concerns regarding this manuscript.

https://doi.org/10.7554/eLife.109518.2.sa1

Author response:

The following is the authors' response to the original reviews

Public Reviews:

Reviewer #1 (Public review):

Summary:

This manuscript by Lin et al. presents a timely, technically strong study that builds patient-specific midbrain-like organoids (MLOs) from hiPSCs carrying clinically relevant GBA1 mutations (L444P/P415R and L444P/RecNcil). The authors comprehensively characterize nGD phenotypes (GCase deficiency, GluCer/GluSph accumulation, altered transcriptome, impaired dopaminergic differentiation), perform CRISPR correction to produce an isogenic line, and test three therapeutic modalities (SapC-DOPS-fGCase nanoparticles, AAV9GBA1, and SRT with GZ452). The model and multi-arm therapeutic evaluation are important advances with clear translational value.

My overall recommendation is that the work undergo a major revision to address the experimental and interpretive gaps listed below.

Strengths:

(1) Human, patient-specific midbrain model: Use of clinically relevant compound heterozygous GBA1 alleles (L444P/P415R and L444P/RecNcil) makes the model highly relevant to human nGD and captures patient genetic context that mouse models often miss.

(2) Robust multi-level phenotyping: Biochemical (GCase activity), lipidomic (GluCer/GluSph by UHPLC-MS/MS), molecular (bulk RNA-seq), and histological (TH/FOXA2, LAMP1, LC3) characterization are thorough and complementary.

(3) Use of isogenic CRISPR correction: Generating an isogenic line (WT/P415R) and demonstrating partial rescue strengthens causal inference that the GBA1 mutation drives many observed phenotypes.

(4) Parallel therapeutic testing in the same human platform: Comparing enzyme delivery (SapC-DOPS-fGCase), gene therapy (AAV9-GBA1), and substrate reduction (GZ452) within the same MLO system is an elegant demonstration of the platform's utility for preclinical evaluation.

(5) Good methodological transparency: Detailed protocols for MLO generation, editing, lipidomics, and assays allow reproducibility

Weaknesses:

(1) Limited genetic and biological replication

(a) Single primary disease line for core mechanistic claims. Most mechanistic data derive from GD2-1260 (L444P/P415R); GD2-10-257 (L444P/RecNcil) appears mainly in therapeutic experiments. Relying primarily on one patient line risks conflating patient-specific variation with general nGD mechanisms.

We thank the reviewer for highlighting the importance of genetic and biological replication. An additional patient-derived iPSC line was included in the manuscript, therefore, our study includes two independent nGD patient-derived iPSC lines, GD2-1260 ($GBA1^{L444P/P415R}$) and GD2-10-257 ($GBA1^{L444P/RecNcil}$), both of which carry the severe mutations associated with nGD. These two lines represent distinct genetic backgrounds and were used to demonstrate the consistency of key disease phenotypes (reduced GCase activity, elevated substrate, impaired dopaminergic neuron differentiation etc.) across different patient's MLOs. Major experiments (e.g., GCase activity assays, substrate, immunoblotting for DA marker TH, and therapeutic testing with SapC-DOPS-fGCase, AAV9-GBA1) were performed using both patient lines, with results showing consistent phenotypes and therapeutic responses (see Figs. 2-6, and Supplementary Figs. 4-5). To ensure clarity and transparency, a new Supplementary Table 2 summarizes the characterization of both, the GD2-1260 and GD2-10-257 lines.

> *(b) Unclear biological replicate strategy. It is not always explicit how many independent differentiations and organoid batches were used (biological replicates vs. technical fields of view).*

Biological replication was ensured in our study by conducting experiments in at least 3 independent differentiations per line, and technical replicates (multiple organoids/fields per batch) were averaged accordingly. We have clarified biological replicates and differentiation in the figure legends.

> *(c) A significant disadvantage of employing brain organoids is the heterogeneity during induction and potential low reproducibility. In this study, it is unclear how many independent differentiation batches were evaluated and, for each test (for example, immunofluorescent stain and bulk RNA-seq), how many organoids from each group were used. Please add a statement accordingly and show replicates to verify consistency in the supplementary data.*

In the revision, we have clarified biological replicates and differentiation in the figure legend in Fig.1E; Fig.2B,2G; Fig.3F, 3G; Fig.4B-C,E,H-J, M-N; Fig.6D; and Fig.7A-C, I.

> *(d) Isogenic correction is partial. The corrected line is WT/P415R (single-allele correction); residual P415R complicates the interpretation of "full" rescue and leaves open whether the remaining pathology is due to incomplete correction or clonal/epigenetic effects.*

We attempted to generate an isogenic iPSC line by correcting both GBA1 mutations (L444P and P415R). However, this was not feasible because GBA1 overlaps with a highly homologous pseudogene (PGBA), which makes precise editing technically challenging. Consequently, only the L444P mutation was successfully corrected, and the resulting isogenic line retains the P415R mutation in a heterozygous state. Because Gaucher disease is an autosomal recessive disorder, individuals carrying a single GBA1 mutation (heterozygous carriers) do not develop clinical symptoms. Therefore, the partially corrected isogenic line, which retains only the P415R allele, represents a clinically relevant carrier model. Consistent with this, our results show that GCase activity was restored to approximately 50% of wild-type levels (Fig.4B-C), supporting the expected heterozygous state. These findings also make it unlikely that the remaining differences observed are due to clonal variation or epigenetic effects.

> *(e) The authors tested week 3, 4, 8, 15, and 28 old organoids in different settings. However, systematic markers of maturation should be analyzed, and different maturation stages should be compared, for example, comparing week 8 organoids to week 28 organoids, with immunofluorescent marker staining and bulk RNAseq.*

We agree that a systematic analysis of maturation stages is essential for validating the MLO model. Our data integrated a longitudinal comparison across multiple developmental windows (Weeks 3 to 28) to characterize the transition from progenitors to mature/functional

states for nGD phenotyping and evaluation of therapeutic modalities: 1) DA differentiation (Wks 3 and 8 in Fig. 3): qPCR analysis demonstrated the progression of DA-specific programs. We observed a steady increase in the mature DA neuron marker *TH* and *ASCL1*. This was accompanied by a gradual decrease in early floor plate/progenitor markers *FOXA2* and *PLZF*, indicating a successful differentiation path from progenitors to differentiated/mature DA neurons. 2) Glycosphingolipid substrates accumulation (Wks 15 and 28 in Fig 2): To assess late-stage nGD phenotyping, we compared GluCer and GluSph at Week 15 and Week 28. This comparison highlights the progressive accumulation of substrates in nGD MLOs, reflecting the metabolic consequences of the disease at different mature stage. 3) Organoid growth dynamics (Wks 4, 8, and 15 in new Fig. 4): The new Fig. 4 tracks physical maturation through organoid size and growth rates across three key time points, providing a macro-scale verification of consistent development between WT and nGD groups. By comparing these early (Wk 3-8) and late (Wk 15-28) stages, we confirmed that our MLOs transition from a proliferative state to a post-mitotic, specialized neuronal state, satisfied the requirement for comparing distinct maturation stages.

> *(f) The manuscript frequently refers to Wnt signaling dysregulation as a major finding. However, experimental validation is limited to transcriptomic data. Functional tests, such as the use of Wnt agonist/inhibitor, are needed to support this claim (see below).*

We agree that the suggested experiments could provide additional mechanistic insights into this study and will consider them in future work.

> *(g) Suggested fixes / experiments*
>
> *Add at least one more independent disease hiPSC line (or show expanded analysis from GD2-10-257) for key mechanistic endpoints (lipid accumulation, transcriptomics, DA markers).*

Additional line iPSC GD2-10-257 derived MLO was included in the manuscript. This was addressed above [see response to Weaknesses (1)-a].

> *Generate and analyze a fully corrected isogenic WT/WT clone (or a P415R-only line) if feasible; at minimum, acknowledge this limitation more explicitly and soften claims.*

We attempted to generate an isogenic iPSC line by correcting both GBA1 mutations (L444P and P415R). However, this was unsuccessful because the GBA1 gene overlaps with a pseudogene (PGBA) located16kd downstream of GBA1, which shares 9698% sequence similarity with GBA1) (Ref#1, #2), which complicates precise editing. GBA1 is shorter (~5.7 kb) than PGBA (~7.6 kb). The primary exonic difference between GBA1 and PGBA is a 55-bp deletion in exon 9 of the pseudogene. As a result, the isogenic line we obtained carries only the P415R mutation, and L444P was corrected to normal sequence. We have included this limitation in the Methods as “This gene editing strategy is expected to also target the GBA1 pseudogene due to the identical target sequence, which limits the gene correction on certain mutations (e.g., P415R)”.

References:

(1) Horowitz M., Wilder S., Horowitz Z., Reiner O., Gelbart T., Beutler E. The human glucocerebrosidase gene and pseudogene: structure and evolution. Genomics (1989). 4, 87–96. doi:10.1016/0888-7543(89)90319-4

(2) Woo EG, Tayebi N, Sidransky E. Next-Generation Sequencing Analysis of GBA1: The Challenge of Detecting Complex Recombinant Alleles. Front Genet. (2021). 12:684067. doi: 10.3389/fgene.2021.684067. PMCID: PMC8255797.

> *Report and increase independent differentiations (N = biological replicates) and present per-differentiation summary statistics.*

This was addressed above [see response to Weaknesses (1)-b, (1)-c].

> *(2) Mechanistic validation is insufficient*
>
> *(a) RNA-seq pathways (Wnt, mTOR, lysosome) are not functionally probed. The manuscript shows pathway enrichment and some protein markers (p-4E-BP1) but lacks perturbation/rescue experiments to link these pathways causally to the DA phenotype.*
>
> *(b) Autophagy analysis lacks flux assays. LC3-II and LAMP1 are informative, but without flux assays (e.g., bafilomycin A1 or chloroquine), one cannot distinguish increased autophagosome formation from decreased clearance.*
>
> *(c) Dopaminergic dysfunction is superficially assessed. Dopamine in the medium and TH protein are shown, but no neuronal electrophysiology, synaptic marker co-localization, or viability measures are provided to demonstrate functional recovery after therapy.*
>
> *(d) Suggested fixes / experiments - Perform targeted functional assays:*
>
> *(i) Wnt reporter assays (TOP/FOP flash) and/or treat organoids with Wnt agonists/antagonists to test whether Wnt modulation rescues DA differentiation.*
>
> *(ii) Test mTOR pathway causality using mTOR inhibitors (e.g., rapamycin) or 4E-BP1 perturbation and assay effects on DA markers and autophagy.*
>
> *Include autophagy flux assessment (LC3 turnover with bafilomycin), and measure cathepsin activity where relevant.*
>
> *Add at least one functional neuronal readout: calcium imaging, MEA recordings, or synaptic marker quantification (e.g., SYN1, PSD95) together with TH colocalization.*

We thank the reviewer for these valuable suggestions. We agree that the suggested experiments could provide additional mechanistic insights into this study and will consider them in future work. Importantly, the primary conclusions of our manuscript, that GBA1 mutations in nGD MLOs resulted in nGD pathologies such as diminished enzymatic function, accumulation of lipid substrates, widespread transcriptomic changes, and impaired dopaminergic neuron differentiation, which can be corrected by several therapeutic strategies in this study, are supported by the evidence presented. The suggested experiments represent an important direction for future research using brain organoids.

> *(3) Therapeutic evaluation needs greater depth and standardization*
>
> *(a) Short windows and limited durability data. SapC-DOPS and AAV9 experiments range from 48 hours to 3 weeks; longer follow-up is needed to assess durability and whether biochemical rescue translates into restored neuronal function.*

We agree with the reviewer. Because this is a proof-of-principle study, the treatment was designed within a short time window. Long-term studies with more comprehensive outcome assessments will be conducted in future work.

> *(b) Dose-response and biodistribution are under-characterized. AAV injection sites/volumes are described, but transduction efficiency, vg copies per organoid, cell-type tropism quantification, and SapC-DOPS penetration/distribution are not rigorously quantified.*

We appreciate the reviewer's concerns. This study was intended to demonstrate the feasibility and initial response of MLOs to AAV therapy. A comprehensive evaluation of AAV biodistribution will be considered in future studies.

The penetration and distribution of SapC-DOPS have been extensively characterized in prior studies. *In vivo* biodistribution of SapC–DOPS coupled CellVue Maroon, a fluorescent cargo, was examined in mice bearing human tumor xenografts using real-time fluorescence imaging, where CellVue Maroon fluorescence in tumor remained for 48 hours (Ref. #3: Fig. 4B, mouse 1), 100 hours (Ref. #4: Fig. 5), up to 216 hours (Ref. #5: Fig. 3). Uptake kinetics were also demonstrated in cells, with flow cytometry quantification showing that fluorescent cargo coupled SapC-DOPS nanovesicles, were incorporated into human brain tumor cell membranes within minutes and remained stably incorporated into the cells for up to one hour (Ref. # 6: Fig. 1a and Fig. 1b). Building on these findings, the present study focuses on evaluating the restoration of GCase function rather than reexamining biodistribution and uptake kinetics.

References:

(3) X. Qi, Z. Chu, Y.Y. Mahller, K.F. Stringer, D.P. Witte, T.P. Cripe. Cancer-selective targeting and cytotoxicity by liposomal-coupled lysosomal saposin C protein. Clin. Cancer Res. (2009) 15, 5840-5851. PMID: 19737950.

(4) Z. Chu, S. Abu-Baker, M.B. Palascak, S.A. Ahmad, R.S. Franco, and X. Qi. Targeting and cytotoxicity of SapC-DOPS nanovesicles in pancreatic cancer. PLOS ONE (2013) 8, e75507. PMID: 24124494.

(5) Z. Chu, K. LaSance, V.M. Blanco, C-H. Kwon, B. Kaur, M. Frederick, S. Thornton, L. Lemen, and X. Qi. Multi-angle rotational optical imaging of brain tumors and arthritis using fluorescent SapC-DOPS nanovesicles. J. Vis. Exp. (2014) 87, e51187, 1-7. PMID: 24837630.

(6) J. Wojton, Z. Chu, C-H. Kwon, L.M.L. Chow, M. Palascak, R. Franco, T. Bourdeau, S. Thornton, B. Kaur, and X. Qi. Systemic delivery of SapC-DOPS has antiangiogenic and antitumor effects against glioblastoma. Mol. Ther. (2013) 21, 1517-1525. PMID: 23732993.

> *(c) Specificity controls are missing. For SapC-DOPS, inclusion of a non-functional enzyme control (or heat-inactivated fGCase) would rule out non-specific nanoparticle effects. For AAV, assessment of off-target expression and potential cytotoxicity is needed.*

Including inactive fGCase would confound the assessment of fGCase in MLOs by immunoblot and immunofluorescence; therefore, saposin C–DOPS was used as the control instead.

We agree that assessment of off-target expression and potential cytotoxicity for AAV is important, this will be included in future studies.

> *(d) Comparative efficacy lacking. It remains unclear which modality is most effective in the long term and in which cellular compartments.*

To address this comment, we have added a new table (Supplementary Table 2) comparing the four therapeutic modalities and summarizing their respective outcomes. While this study focused on short-term responses as a proof-of-principle, future work will explore long-term therapeutic effects.

> *(e) Suggested fixes/experiments*
>
> *Extend follow-up (e.g., 6+ weeks) after AAV/SapC dosing and evaluate DA markers, electrophysiology, and lipid levels over time.*

We appreciate the reviewer's suggestions. The therapeutic testing in patient-derived MLOs was designed as a proof-of-principle study to demonstrate feasibility and the primary response (rescue of GCase function) to the treatment. A comprehensive, long-term therapeutic evaluation of AAV and SapC-DOPS-fGCase is indeed important for a complete assessment; however, this represents a separate therapeutic study and is beyond the scope of the current work.

> *Quantify AAV transduction by qPCR for vector genomes and by cell-type quantification of GFP+ cells (neurons vs astrocytes vs progenitors).*

For the AAV-treated experiments, we agree that measuring AAV copy number and GFP expression would provide additional information. However, the primary goal of this study was to demonstrate the key therapeutic outcome, rescue of GCase function by AAV-delivered normal GCase, which is directly relevant to the treatment objective.

> *Include SapC-DOPS control nanoparticles loaded with an inert protein and/or fluorescent cargo quantitation to show distribution and uptake kinetics.*

As noted above [see response to Weakness (3)-c], using inert GCase would confound the assessment of fGCase uptake in MLOs; therefore, it was not suitable for this study. See response above for the distribution and uptake kinetics of SapC-DOPS [see response to Weaknesses (3)-b].

> *Provide head-to-head comparative graphs (activity, lipid clearance, DA restoration, and durability) with statistical tests.*

We have added a new table (Supplementary Table 2) providing a head-to-head comparison of the treatment effects.

> *(4) Model limitations not fully accounted for in interpretation*
>
> *(a) Absence of microglia and vasculature limits recapitulation of neuroinflammatory responses and drug penetration, both of which are important in nGD. These absences could explain incomplete phenotypic rescues and must be emphasized when drawing conclusions about therapeutic translation.*

We agree that the absence of microglia and vasculature in midbrain-like organoids represents a limitation, as we have discussed in the manuscript. In this revision, we highlighted this limitation in the Discussion section and clarified that it may contribute to incomplete phenotyping and phenotypic rescue observed in our therapeutic experiments. Additionally, we have outlined future directions to incorporate microglia and vascularization into the organoid system to better recapitulate the in vivo environment and improve translational relevance (see 7th paragraph in the Discussion).

> *(b) Developmental vs degenerative phenotype conflation. Many phenotypes appear during differentiation (patterning defects). The manuscript sometimes interprets these as degenerative mechanisms; the distinction must be clarified.*

We appreciate the reviewer's comments. In the revised manuscript, we have clarified that certain abnormalities, such as patterning defects observed during early differentiation, likely reflect developmental consequences of GBA1 mutations rather than degenerative processes. Conversely, phenotypes such as substrate accumulation, lysosomal dysfunction, and impaired dopaminergic maturation at later stages are interpreted as degenerative features. We have updated the Results and Discussion sections to avoid conflating developmental defects with neurodegenerative mechanisms.

> *(c) Suggested fixes*

> *Tone down the language throughout (Abstract/Results/Discussion) to avoid overstatement that MLOs fully recapitulate nGD neuropathology.*

The manuscript has been revised to avoid overstatements.

> *Add plans or pilot data (if available) for microglia incorporation or vascularization to indicate how future work will address these gaps.*

The manuscript now includes further plans to address the incorporation of microglia and vascularization, described in the last two paragraphs in the Discussion. Pilot study of microglia incorporation will be reported when it is completed.

> *(5) Statistical and presentation issues*
>
> *(a) Missing or unclear sample sizes (n). For organoid-level assays, report the number of organoids and the number of independent differentiations.*

We have clarified biological replicates and differentiation in the figure legend [see response to Weaknesses (1)-b, (1)-c].

> *(b) Statistical assumptions not justified. Tests assume normality; where sample sizes are small, consider non-parametric tests and report exact p-values.*

We have updated Statistical analysis in methods as described below:

For comparisons between two groups, data were analyzed using unpaired two-tailed Student's t-tests when the sample size was ≥6 per group and normality was confirmed by the Shapiro-Wilk test. When the normality assumption was not met or when sample sizes were small ($n < 6$), the non-parametric Mann-Whitney U test was used instead. For comparisons involving three or more groups, one-way ANOVA followed by Tukey's multiple comparison test was applied when data were normally distributed; otherwise, the nonparametric Dunn's multiple comparison test was used. Exclusion of outliers was made based on cutoffs of the mean ±2 standard deviations. All statistical analyses were performed using GraphPad Prism 10 software. Exact p-values are reported throughout the manuscript and figures where feasible. A p-value < 0.05 was considered statistically significant.

> *(c) Quantification scope. Many image quantifications appear to be from selected fields of view, which are then averaged across organoids and differentiations.*

In this work, quantitative immunofluorescence analyses (e.g., cell counts for FOXP1+, FOXG1+, SOX2+ and Ki67+ cells, as well as marker colocalization) were performed on at least 3–5 randomly selected non-overlapping fields of view (FOVs) per organoid section, with a minimum of 3 organoids per differentiation batch. Each FOV was imaged at consistent magnification (60x) and z-stack depth to ensure comparable sampling across conditions. Data from individual FOVs were first averaged within each organoid to obtain an organoid-level mean, and then biological replicates (independent differentiations, $n \geq 3$) were averaged to generate the final group mean ± SEM. This multilevel averaging approach minimizes bias from regional heterogeneity within organoids and accounts for variability across differentiations. Representative confocal images shown in the figures were selected to accurately reflect the quantified data. We believe this standardized quantification strategy ensures robust and reproducible results while appropriately representing the 3D architecture of the organoids.

In the revision, we have clarified the method used for image analysis of sectioned MLOs as below:

Quantitative immunofluorescence analyses (e.g., cell counts for FOXP1+, FOXG1+, SOX2+ and Ki67+ cells, as well as marker colocalization) were performed using ImageJ (NIH) on at least 3–5 randomly selected non-overlapping fields of view (FOVs) per organoid section, with a minimum of 3 organoids per differentiation batch. Each FOV was imaged at consistent magnification (60x) and z-stack depth to ensure comparable sampling across conditions. Data from individual FOVs were first averaged within each organoid to obtain an organoid-level mean, and then biological replicates (independent differentiations, n ≥ 3) were averaged to generate the final group mean ± SEM.

> *(d) RNA-seq QC and deposition. Provide mapping rates, batch correction details, and ensure the GEO accession is active. Include these in Methods/Supplement.*

RNA-seq data are from same batch. The mapping rate is >90%. GEO accession will be active upon publication. These were included in the Methods.

> *(e) Suggested fixes*
>
> *Add a table summarizing biological replicates, technical replicates, and statistical tests used for each figure panel.*

We have revised the figure legends to include replicates for each figure and statistical tests [see response in weaknesses (1)-b, (1)-c].

> *Recompute statistics where appropriate (non-parametric if N is small) and report effect sizes and confidence intervals.*

Statistical analysis method is provided in the revision [see response in Weaknesses (5)-b].

> *(6) Minor comments and clarifications*
>
> *(a) The authors should validate midbrain identity further with additional regional markers (EN1, OTX2) and show absence/low expression of forebrain markers (FOXG1) across replicates.*

We validated the MLO identity by 1) FOXG1 and 2) EN1. FOXG1 was barely detectable in Wk8 75.1_MLO but highly present in 'age-matched' cerebral organoid (CO), suggesting our culturing method is midbrain region-oriented. In nGD MLO, FOXG1 expression is significantly higher than 75.1_MLO, indicating that there was aberrant anterior-posterior brain specification, consistent with the transcriptomic dysregulation observed in our RNA-seq data.

To further confirm midbrain identity, we examined the expression of EN1, an established midbrain-specific marker. Quantitative RT-PCR analysis demonstrated that EN1 expression increased progressively during differentiation in both WT-75.1 and nGD2-1260 MLOs at weeks 3 and 8 (Author response image 1). EN1 reached 34-fold and 373-fold higher levels than in WT-75.1 iPSCs at weeks 3 and 8, respectively, in WT-75.1 MLOs. In nGD MLOs, although EN1 expression showed a modest reduction at week 8, the levels were not significantly different from those observed in age-matched WT-75.1 MLOs ($p > 0.05$, ns).

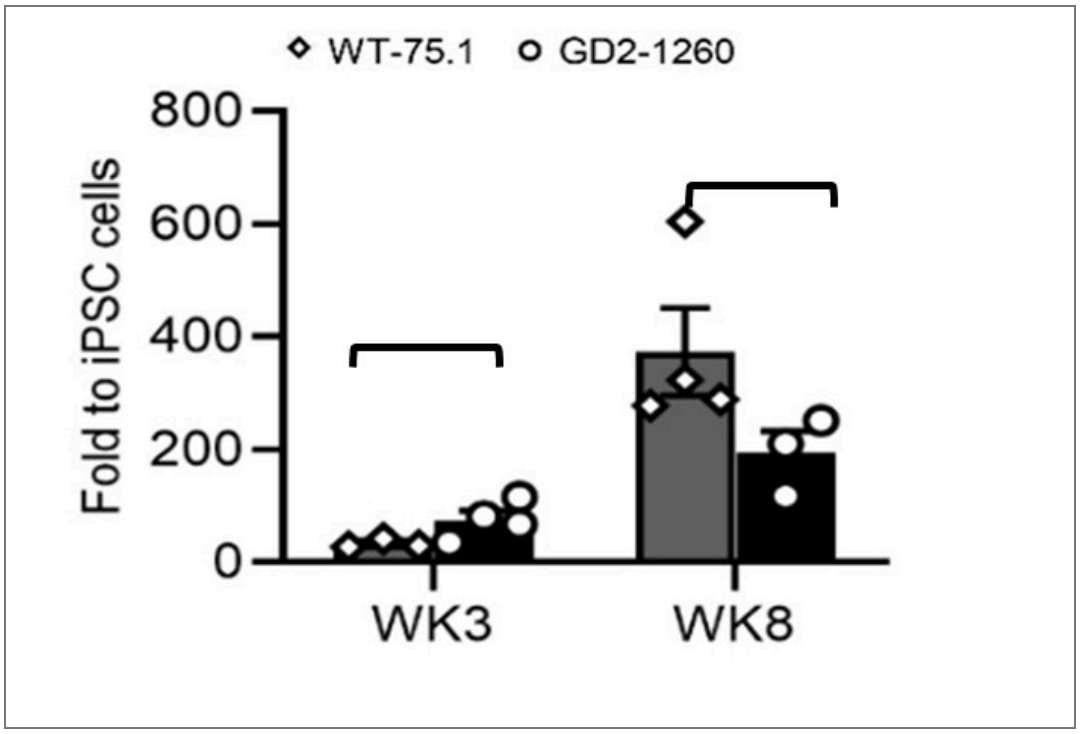

Author response image 1. qRT-PCR quantification of midbrain progenitor marker *EN1* expression in WT-75. 1 and GD2-1260 MLOs at Wk3 and Wk8. Data was normalized to WT-75.1 hiPSC cells and presented as mean ± SEM (n = 3-4 MLOs per group). ns, not significant.

> *(b) Extracellular dopamine ELISA should be complemented with intracellular dopamine or TH+ neuron counts normalized per organoid or per total neurons.*

We quantified TH expression at both the mRNA level (Fig. 3F) and the protein level (Fig. 3G/H) from whole-organoid lysates, which provides a more consistent and integrative measure across samples. These TH expression levels correlated well with the corresponding extracellular (medium) dopamine concentrations for each genotype. In contrast, TH^+ neuron counts may not reliably reflect total cellular dopamine levels because the number of cells captured on each organoid section varies substantially, making normalization difficult. Measuring intracellular dopamine is an alternative approach that will be considered in future studies.

> *(c) For CRISPR editing: the authors should report off-target analysis (GUIDE-seq or targeted sequencing of predicted off-targets) or at least in-silico off-target score and sequencing coverage of the edited locus. (off-target analysis (GUIDE-seq or targeted sequencing of predicted off-targets) or at least in-silico off-target score and sequencing coverage of the edited locus).*

The off-target effect was analyzed during gene editing and the chance to target other off-targets is low due to low off-target scores ranked based on the MIT Specificity Score analysis. The related method was also updated as stated below:

"The chance to target other off-targets is low due to low off-target scores ranked based on the MIT Specificity Score analysis (Hsu, P., Scott, D., Weinstein, J. et al. DNA targeting specificity of RNA-guided Cas9 nucleases. Nat Biotechnol 31, 827–832 (2013). (*https://doi.org/10.1038/nbt.2647*)."

> *(d) It should be clarified as to whether lipidomics normalization is to total protein per organoid or per cell, and include representative LC-MS chromatograms or method QC.*

The normalization was to the protein of organoid lysate. This was clarified in the Methods section in the revision as stated below:

"The GluCer and GluSph levels in MLO were normalized to total MLO protein (mg) that were used for glycosphingolipids analyses. Protein mass was determined by BCA assay and glycosphingolipid was expressed as pmol/mg protein. Additionally, GluSph levels in the culture medium were quantified and normalized to the medium volume (pmol/mL)."

Representative LC-MS chromatograms for both normal and GD MLOs have been included in a new figure, Supplementary Figure 2.

> *(e) Figure legends should be improved in order to state the number of organoids, the number of differentiations, and the exact statistical tests used (including multiplecomparison corrections).*

This was addressed above [see response to Weaknesses (1)-b and (5)-b].

> *(f) In the title, the authors state "reveal disease mechanisms", but the studies mainly exhibit functional changes. They should consider toning down the statement.*

The title was revised to: Patient-Specific Midbrain Organoids with CRISPR Correction Recapitulate Neuronopathic Gaucher Disease Phenotypes and Enable Evaluation of Novel Therapies

> *(7) Recommendations*
>
> *This reviewer recommends a major revision. The manuscript presents substantial novelty and strong potential impact but requires additional experimental validation and clearer, more conservative interpretation. Key items to address are:*
>
> *(a) Strengthening genetic and biological replication (additional lines or replicate differentiations).*

This was addressed above [see response to Weaknesses (1)-a, (1)-b, (1)-c].

> *(b) Adding functional mechanistic validation for major pathways (Wnt/mTOR/autophagy) and providing autophagy flux data.*
>
> *(c) Including at least one neuronal functional readout (calcium imaging/MEA/patch) to demonstrate functional rescue.*

As addressed above [see response to Weaknesses (2)], the suggested experiments in b) and c) would provide additional insights into this study and we will consider them in future work.

> *(d) Deepening therapeutic characterization (dose, biodistribution, durability) and including specificity controls.*

This was addressed above [see response to Weaknesses (3)-a to e].

> *(e) Improving statistical reporting and explicitly stating biological replicate structure.*

This was addressed above [see response to Weaknesses (1)-b, (5)-b].

> ***Reviewer #2 (Public review):***
>
> *Sun et al. have developed a midbrain-like organoid (MLO) model for neuronopathic Gaucher disease (nGD). The MLOs recapitulate several features of nGD molecular pathology, including reduced GCase activity, sphingolipid accumulation, and impaired dopaminergic neuron development. They also characterize the transcriptome in the MLO*

> *nGD model. CRISPR correction of one of the GBA1 mutant alleles rescues most of the nGD molecular phenotypes. The MLO model was further deployed in proof-of-principle studies of investigational nGD therapies, including SapC-DOPS nanovesicles, AAV9-mediated GBA1 gene delivery, and substrate-reduction therapy (GZ452). This patient-specific 3D model provides a new platform for studying nGD mechanisms and accelerating therapy development. Overall, only modest weaknesses are noted.*

We thank the reviewer for the supportive remarks.

> ***Reviewer #3 (Public review):***
>
> *Summary:*
>
> *In this study, the authors describe modeling of neuronopathic Gaucher disease (nGD) using midbrain-like organoids (MLOs) derived from hiPSCs carrying GBA1 L444P/P415R or L444P/RecNciI variants. These MLOs recapitulate several disease features, including GCase deficiency, reduced enzymatic activity, lipid substrate accumulation, and impaired dopaminergic neuron differentiation. Correction of the GBA1 L444P variant restored GCase activity, normalized lipid metabolism, and rescued dopaminergic neuronal defects, confirming its pathogenic role in the MLO model. The authors further leveraged this system to evaluate therapeutic strategies, including: (i) SapC-DOPS nanovesicles for GCase delivery, (ii) AAV9-mediated GBA1 gene therapy, and (iii) GZ452, a glucosylceramide synthase inhibitor. These treatments reduced lipid accumulation and ameliorated autophagic, lysosomal, and neurodevelopmental abnormalities.*
>
> *Strengths:*
>
> *This manuscript demonstrates that nGD patient-derived MLOs can serve as an additional platform for investigating nGD mechanisms and advancing therapeutic development.*
>
> *Comments:*
>
> *(1) It is interesting that GBA1 L444P/P415R MLOs show defects in midbrain patterning and dopaminergic neuron differentiation (Figure 3). One might wonder whether these abnormalities are specific to the combination of L444P and P415R variants or represent a general consequence of GBA1 loss. Do GBA1 L444P/RecNciI (GD2-10-257) MLOs also exhibit similar defects?*

We observed reduced dopaminergic neuron marker TH expression in GBA1 L444P/RecNciI (GD2-10-257) MLOs, suggesting that this line also exhibits defects in dopaminergic neuron differentiation. These data are provided in a new Supplementary Fig. 4E, and are summarized in new Supplementary Table 2 in the revision.

> *(2) In Supplementary Figure 3, the authors examined GCase localization in SapC-DOPSfGCase-treated nGD MLOs. These data indicate that GCase is delivered to TH^+ neurons, $GFAP^+$ glia, and various other unidentified cell types. In fruit flies, the GBA1 ortholog, Gba1b, is only expressed in glia (PMID: 35857503; 35961319). Neuronally produced GluCer is transferred to glia for GBA1-mediated degradation. These findings raise an important question: in wild-type MLOs, which cell type(s) normally express GBA1? Are they dopaminergic neurons, astrocytes, or other cell types?*

All cell types in wild-type MLOs are expected to express GBA1, as it is a housekeeping gene broadly expressed across neurons, astrocytes, and other brain cell types. Its lysosomal function is essential for cellular homeostasis and is therefore not restricted to any specific lineage. (*https://www.proteinatlas.org/ENSG00000177628GBA1/brain/midbrain*).

> *(3) The authors may consider switching Figures 2 and 3 so that the differentiation defects observed in nGD MLOs (Figure 3) are presented before the analysis of other phenotypic*

> *abnormalities, including the various transcriptional changes (Figure 2).*

We appreciate the reviewer's suggestion; however, we respectfully prefer to retain the current order of Figures 2 and 3, as we believe this structure provides the clearest narrative flow. Figure 2 establishes the core biochemical hallmarks: reduced GCase activity, substrate accumulation, and global transcriptomic dysregulation (1,429 DEGs enriched in neural development, WNT signaling, and lysosomal pathways), which together provide essential molecular context for studying the specific cellular differentiation defects presented in Figure 3. Presenting the broader disease landscape first creates a coherent mechanistic link to the subsequent analyses of midbrain patterning and dopaminergic neuron impairment.

To enhance readability, we have added a brief transitional sentence at the start of the Figure 3 paragraph: "Building on the molecular and transcriptomic hallmarks of GCase deficiency observed in nGD MLOs (Figure 2), we next investigated the impact on midbrain patterning and dopaminergic neuron differentiation (Figure 3)."

> ***Recommendations for the authors:***
>
> ***Reviewing Editor Comments:***
>
> *Your paper has been reviewed by three expert reviewers in the GBA field. Although they appreciate the work and its novelty, they raise several concerns. We suggest that you to address these concerns in the next version.*
>
> ***Reviewer #1 (Recommendations for the authors):***
>
> *Statistical and presentation issues*
>
> *(1) Missing or unclear sample sizes (n). For organoid-level assays, report the number of organoids and the number of independent differentiations.*

This was addressed above [see response to Reviewer 1 Weaknesses (1)- b].

> *(2) Statistical assumptions not justified. Tests assume normality; where sample sizes are small, consider non-parametric tests and report exact p-values.*

We have updated methods to describe the Statistical analysis details [see response to Reviewer 1 Weaknesses (5)-b].

> *(3) Quantification scope. Many image quantifications appear to be from selected fields of view, which are then averaged across organoids and differentiations.*

This was addressed above [see response to Reviewer 1 Weaknesses (5)- c].

> *(4) RNA-seq QC and deposition. Provide mapping rates, batch correction details, and ensure the GEO accession is active. Include these in Methods/Supplement.*

Our RNA-seq data were generated from a single batch of MLOs, with mapping rates exceeding 90%. The GEO accession will be made publicly available upon publication.

> ***Reviewer #2 (Recommendations for the authors):***
>
> *Please consider the following suggestions for revisions:*
>
> *(1) Line 86: A bit more explanation/justification for the focus on midbrain-like organoids would be helpful, including introducing the nature of the midbrain pathology to better put some of the MLO findings in context. Is the nGD pathology for the midbrain significantly different / out of proportion to other affected brain regions?*

nGD Patients often display impaired vertical gaze and movement disorders. These symptoms correlate with midbrain involvement due to the sensitivity of this region to neuroinflammatory and degenerative processes (Ref #7, #8). Both human and mouse studies indicate that the midbrain exhibits prominent substrate accumulation compared to other brain regions, suggesting a predisposition for greater pathological involvement in GD midbrain (Ref #8, #9, #10, #11). This rationale was added to Line 86 in the revision.

References:

(7) Goker-Alpan O, Ivanova MM. Neuronopathic Gaucher disease: Rare in the West, common in the East. J Inherit Metab Dis.(2024) 47(5):917-934. PMID: 38768609.

(8) Burrow TA, Sun Y, Prada CE, Bailey L, Zhang W, Brewer A, Wu SW, Setchell KDR, Witte D, Cohen MB, Grabowski GA. CNS, lung, and lymph node involvement in Gaucher disease type 3 after 11 years of therapy: clinical, histopathologic, and biochemical findings. Mol Genet Metab. (2015) 114(2):233-241. PMID: 25219293.

(9) Tamar Farfel-Becker, Einat B. Vitner, Samuel L. Kelly, Jessica R. Bame, Jingjing Duan, Vera Shinder, Alfred H. Merrill, Kostantin Dobrenis, Anthony H. Futerman. Neuronal accumulation of glucosylceramide in a mouse model of neuronopathic Gaucher disease leads to neurodegeneration, Human Molecular Genetics, (2014). Volume 23, Issue 4, Pages 843–854.

(10) E. Ellen Jones, Wujuan Zhang, Xueheng Zhao, Cristine Quiason , Stephanie Dale, Sheerin Shahidi-Latham, Gregory A. Grabowski, Kenneth D. R. Setchell, Richard R. Drake, and Ying Sun. High-Resolution MALDI Imaging Mass Spectrometry. SLAS Discovery (2017). Vol. 22(10) 1218–1228

(11) Xu YH, Xu K, Sun Y, Liou B, Quinn B, Li RH, Xue L, Zhang W, Setchell KD, Witte D, Grabowski GA. Multiple pathogenic proteins implicated in neuronopathic Gaucher disease mice. Hum Mol Genet. (2014) 23(15):3943-57. PMID: 24599400.

> *(2) Lines 359-360: Please specify the carbon-chain length of the sphingoid base of the GluCer species analyzed. Also, is there a citation for the statement that 18:0 and 16:0 are "brain-enriched species"?*

The carbon-chain length analyzed ranges from 14:0 to 24:0. The sphingoid base for all GluCer species analyzed is d18:1. For example, the species referred to as GluCer 18:0 corresponds to GluCer(d18:1/18:0). Although both, 16:0 and 18:0 are enriched in the brain, 18:0 is the most abundant species in the brain (Ref #12, #13). We revised "brain-enriched species" to “brain-predominant species (18:0)”.

References:

(12) Nilsson, O., and Svennerholm, L. Accumulation of Glucosylceramide and Glucosylsphingosine (Psychosine) in Cerebrum and Cerebellum in Infantile and Juvenile Gaucher Disease. Journal of Neurochemistry (1982) 39, 709–718.

(13) Sun, Y., Zhang, W., Xu, Y.H., Quinn, B., Dasgupta, N., Liou, B., Setchell, K.D., and Grabowski, G.A. Substrate compositional variation with tissue/region and Gba1 mutations in mouse models--implications for Gaucher disease. PLoS One (2013). 8, e57560.10.1371/journal.pone.0057560.

> *(3) Figure 2: It would be interesting to compare the MLO findings to prior gene expression data. Are there previously published transcriptome analyses from nGD brain tissue (or other tissues) that the transcriptome data obtained from MLOs may be compared with? What about transcriptome analyses of mouse GD models?*

We thank the reviewer for this valuable suggestion. To strengthen the biological context of our transcriptomic findings, we have added a new comparative table (new Supplementary Table 3) in the revised manuscript that summarizes key dysregulated pathways in our human nGD MLOs alongside previously published data from nGD mouse midbrain (Ref#14). The table highlights substantial overlap, including axon guidance, neuron differentiation, dopaminergic/glutamatergic/GABAergic synaptic signaling, lipid metabolism, apoptosis/cell death, and nervous system development, emphasizing the translational relevance of our model. We also note that our dataset uniquely reveals pronounced dysregulation of WNT signaling and anterior-posterior patterning (Fig. 2L and 2M), potentially reflecting human-specific early midbrain defects.

We added the following sentence to Discussion: "Comparative analysis with prior transcriptomic data from nGD mouse midbrain showed consistent dysregulation in axon guidance, synaptic signaling, lipid metabolism, and nervous system development (new Supplementary Table 3), supporting the fidelity of our human MLO model."

Reference:

(14) Dasgupta N, Xu YH, Li R, Peng Y, Pandey MK, Tinch SL, Liou B, Inskeep V, Zhang W, Setchell KD, Keddache M, Grabowski GA, Sun Y. Neuronopathic Gaucher disease: dysregulated mRNAs and miRNAs in brain pathogenesis and effects of pharmacologic chaperone treatment in a mouse model. Hum Mol Genet. (2015) 24(24):7031-48. PMID: 26420838.

> *(4) Lines 402-405 & Figure 3D: Is it possible to include a merged image to better visualize the TH and FOXA2 co-staining / potential colocalization?*

The merged images of TH (red) and FOXA2 (green) are shown in Fig. 3E. Yellow arrows indicate TH and FOXA2 co-stained cells, which appear yellow in the merged images. The results demonstrate that the number of co-stained cells is reduced in GD2-1260 MLOs compared with WT-75.1 MLOs at both, week 6 and week 8.

> *(5) Lines 447-448 & Figure 4F, G, J: It would be helpful to provide a direct analysis/visualization of MLO size between the WT-75.1, GD2-1260, and iso-GD2-1260 genotypes (allowing direct comparison of WT and iso). Similarly, the same 3-way analysis would be valuable for assessing dopamine levels.*

We have included WT-75.1 in Fig. 4 F/G/J in the revision. All three genotypes, WT-75.1, GD2-1260, and iso-GD2-1260, are presented for analysis compared to WT-75.1. In new Figure 4F, MLO growth is presented by representative MLO images taken under wide field microscopy at day 2, Wk4 and Wk8 of differentiation. In new Fig. 4G, MLOs size was analyzed by NIS elements and presented as the area (μm^2) of MLO in image (mean ± SEM). N≥10 MLOs were analyzed for each genotype. In new Fig. 4J. Dopamine levels in MLO culture medium from WT-75.1, GD2-1260 and iso- GD2-1260 MLOs at Wk12 cultured in 3 mL BGM medium for 72 hours were analyzed. Data are presented as mean ± SEM (n = 5 per group). Statistical analysis applied was described in the legend.

> *(6) Figure 4: What is the explanation/interpretation of the residual autophagy pathway dysfunction in CRISPR-corrected MLOs? nGD requires near-complete loss of GCase activity, so it is a bit curious that autophagic dysfunction would be observed with only ~50% GCase reduction? There is some discussion, but it doesn't fully capture the unexpected nature and implications of this result.*

This phenomenon may be explained by a threshold effect in lysosomal function. Gaucher disease is an autosomal recessive disorder. The carriers with heterozygous GBA1 mutation, who retain approximately 50% of normal GCase activity, do not develop disease. This suggests that even partial restoration of GCase activity can reduce glucosylceramide accumulation

below a pathological threshold, thereby restoring lysosomal integrity and autophagic flux. In addition, improved GCase activity may help normalize the lipid composition of lysosomal membranes, facilitating the fusion events required for effective autophagy.

> *(7) Lines 512-516 & Figure 5J: The data shown are inconclusive. Can these Western blot data be quantified, noting the number of replicates for each measurement? Without quantification and statistics, it is difficult to assess the claim that levels of LAMP1, LC3-I, LC3-II, 4E-BP1, and p-4E-BP1 in GD2-1260 treated with SapC-DOPS-fGCase are more similar to GD2-1260 treated following SapC-DOPS than to WT-75.1.*

We performed quantitative analysis by comparing WT-75.1 and included the data in new Fig. 5J. The result was revised as:

Analysis of protein levels showed that decreased LAMP1 expression in GD2 1260 MLOs was not altered following SapC DOPS fGCase treatment (Figure 5J). The elevated LC3-II levels, an indicator of impaired autophagic flux, were reduced upon treatment, suggesting enhanced autophagic activity (Figure 5J). Moreover, phosphorylated 4E-BP1 (Thr37/46), but not total 4E-BP1, was improved in SapC-DOPS-fGCase–treated MLOs, reflecting a decrease in mTOR hyperactivation (Figure 5J). We anticipate that a longer duration of SapC-DOPS-fGCase exposure in nGD MLOs may produce a more robust therapeutic effect in rescuing nGD-associated phenotypes, which will be evaluated in future studies.

> *(8) Lines 518-520: The presented data support "effective restoration of GCase activity," but clarification is needed regarding "correction of GD-related disease phenotypes." Perhaps "selected molecular and biochemical phenotypes" would be more accurate. Data are not shown for several other phenotypes, including TH, FOXA2, and dopamine levels.*

This was revised to “selected molecular and biochemical phenotypes “.

> *(9) Figure 5D-J: Please clarify whether all experiments were conducted 48 hours after treatment, as indicated for Figure 5C. If so, does this suggest that SapC-DOPS treatment exhibits only short-term effects? Were any data collected to evaluate the persistence of the treatment effect?*

The treatment duration is specified in the Fig. 5 legend. Fig. 5D–J represent experiments conducted after two weeks of treatment, whereas Fig. 5C reflects a 48-hour treatment. In both Gaucher disease lines, two-week treatment restored GCase activity to wild-type levels and reduced GluSph substrate accumulation. These findings were intended as proof-of-principle to demonstrate therapeutic feasibility; evaluation of treatment persistence beyond two weeks was beyond the scope of this study.

> *Minor suggestions*
>
> *(1) Line 80: "A brain organoid derived from hiPSCs of a healthy individual with GBA1 knockout and α-synuclein overexpression exhibited some PD features23." I would suggest enumerating what "PD features" are to distinguish from "clinical features", which I don't think is the intended meaning.*

This was revised as “exhibited characteristic PD markers”.

> *(2) Figure 2I: The reported number of downregulated DEGs is incorrect. It should be 765, not 1429.*

This was corrected in Figure 2I.

> *(3) Line 359: change "enrich" to "enriched".*

This word was corrected.

https://doi.org/10.7554/eLife.109518.2.sa0